ENVIRONMENTAL RESEARCH
COMMUNICATIONS

INCLUSIVE PUBLISHING
TRUSTED SCIENCE

Part of the
ENVIRONMENTAL RESEARCH
SERIES

PURPOSE-LED
PUBLISHING™

LETTER • **OPEN ACCESS**

Forecasting austral summer precipitation along the western coast of South America (WCSA)

To cite this article: Juan Sulca and Ken Takahashi 2025 *Environ. Res. Commun.* **7** 101005

Environmental Research Communications

OPEN ACCESS

RECEIVED
3 June 2024

REVISED
1 September 2025

ACCEPTED FOR PUBLICATION
30 September 2025

PUBLISHED
15 October 2025

LETTER

Forecasting austral summer precipitation along the western coast of South America (WCSA)

Juan Sulca[1,2,*] **and Ken Takahashi**[1]

[1] Ciencias de la Atmósfera, Hidrósfera y Cambio Climático, Instituto Geofísico del Perú, Lima, Peru
[2] Facultad de Ciencias, Universidad Nacional de Ingeniería, Lima, Peru
[*] Author to whom any correspondence should be addressed.

E-mail: sulcaf5@gmail.com

Keywords: coast of northern Peru and Ecuador, multiple linear regression (MLR) model, Central and Eastern El Niño, Central and East Pacific ITCZ, The GFDL-SPEAR model, precipitation, austral summer

Abstract

Forecasting precipitation could help prevent flooding and drought disasters along the western coast of South America (WCSA), stretching from northern Peru to Ecuador. This study constructed a multiple linear regression (MLR) model to forecast precipitation anomalies with high spatial resolution across WCSA during the austral summer (December-January-February, DJF) for the period 1982–2023. The predictors of the MLR model are the central and eastern Pacific El Niño (C and E) and the central and east Pacific Intertropical Convergence Zone (CPITCZ and EPITCZ) indices. Furthermore, we readjusted the MLR model using forecasts from the Geophysical Fluid Dynamic Model (GFDL) model from the Seamless System for prediction and Earth System Research (SPEAR) called the GFDL-SPEAR ($MLR_{GFDL\text{-}SPEAR}$) as predictors. The MLR model predicts DJF precipitation anomalies across WCSA because the E, CPITCZ and EPITCZ indices strongly correlate with DJF WCSA precipitation due to their influence on atmospheric circulation to trigger deep convection over far-eastern Pacific Ocean. The MLR_{OBS} model exhibits the highest performance over most WCSA ($r > 0.6$, $p < 0.05$), except along the coast of Ecuador and the Peru-Ecuador border by present high root mean square error values (above 20 mm month^{-1}). The GFDL-SPEAR model provides more accurate forecasts of the DJF time series for the CPITCZ index than for the E and EPITCZ indices, due to Central Pacific ITCZ responses linearly to warm SST anomalies over western Pacific Ocean and it realistically simulates DJF precipitation patterns over Southern Pacific Ocean and Peru.

1. Introduction

The western coast of South America (WCSA, figure 1) stretches along the northwestern part of the continent, bordered by the Pacific Ocean and the Andes Mountains, spanning from the northern coast of Peru to the coast of Ecuador (8.75°S-0.75°N, 79–81.75°W). Despite being an arid and narrow region, the WCSA has important economic activities such as fishing and intensive agriculture of rice, grapes, and mangoes. Climatologically, the coasts of northern Peru and Ecuador experience distinct rainy seasons. In northern Peru, the rainy season typically spans from late December to April (Rau *et al* 2017). Similarly, on the Ecuadorian coast, this rainy season typically occurs between January and April (Ilbay-Yupa *et al* 2021).

The El Niño-Southern Oscillation (ENSO) is widely acknowledged as the principal interannual pattern affecting sea surface temperature (SST) in the equatorial Pacific Ocean. ENSO influences global precipitation and temperature by modifying large-scale atmospheric circulation patterns (Ropelewski and Halpert 1987, Trenberth *et al* 1998). The warm phase of ENSO is termed El Niño, while the cold phase is referred to as La Niña. Moreover, both El Niño and La Niña phases often intensify extreme precipitation and temperature events, especially during their peak periods from November to January or February. For instance, El Niño

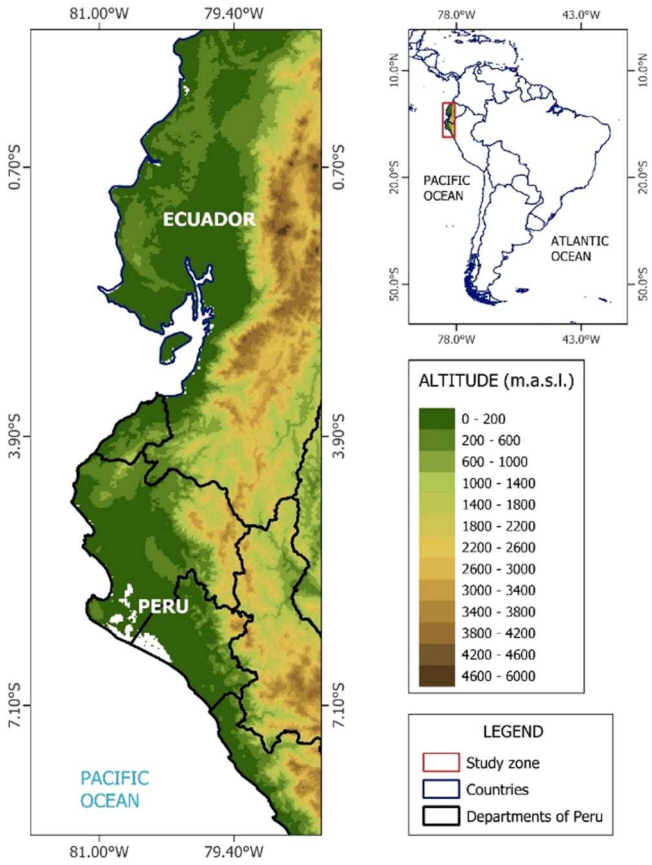

Figure 1. Location of the western coast of South America (WCSA). The green shadings represent the topographic elevation of the western coast of South America.

induces heavy precipitation across much of the WCSA (Takahashi 2004, Lagos *et al* 2008, Lavado-Casimiro and Espinoza 2014, Recalde-Coronel *et al* 2014, De Guenni *et al* 2017, Tobar and Wyseure 2018, Sulca *et al* 2018, Sanabria *et al* 2018, Thielen *et al* 2023), except the southernmost Ecuadorian coast (Ilbay-Yupa *et al* 2021). Precipitation intensifies and frequently lingers during Extraordinary El Niño events, leading to significant floodings, economic losses and the loss of numerous lives, as observed in 1982/83 and 1997/98 (Waylen and Caviedes 1986, World Bank 2014). Conversely, the opposite scenario may not necessarily occur during La Niña events.

Various indices have been developed to quantify and diagnose the El Niño events to mitigate their impacts in WCSA. For example, the Southern Oscillation Index (SOI) is an large-scale atmospheric index. The Niño1 + 2 and Niño3 indices are based on the average of the SST anomalies inside regions located in the eastern equatorial Pacific Ocean. Additionally, the Multivariate ENSO Index (MEI) is calculated as a combination of the above-mentioned indices using multiple linear regression techniques (Wolter and Timlin 1993). In recent decades, several proposals have been made it to consider pairs of indices to describe ENSO diversity (Ashok *et al* 2007, Capotondi *et al* 2015, 2020, Cai *et al* 2021), such as Takahashi *et al* (2011), who proposed two indices known as the central and eastern Pacific El Niño SST (C and E) indices, which represent the SST variability over the central and eastern equatorial Pacific, to describe the nonlinear behavior of El Niño. Lavado-Casimiro and Espinoza (2014) and Sulca *et al* (2018) reported that the warm E phase induces precipitation along the northern Peru and Ecuador coasts during the austral summer, while the warm C phase is not correlated with the austral summer (December-January-February, DJF) precipitation in these coastal regions themselves, but higher up the Andes.

The Inter-Tropical Convergence Zone (ITCZ) is a band of deep convective cloud as consequence of the convergence of trade winds over warm tropical waters along the equatorial belt. The cold water west of the South American coast is strongly associated with the ITCZ being mainly located in the Northern Hemisphere in the east Pacific (Philander *et al* 1996, Takahashi and Battisti 2007). During extreme El Niño episodes in the eastern Pacific, a single strong East Pacific ITCZ (hereafter EPITCZ) is present south of the equator (e.g. Huaman and Takahashi 2016). In addition, the EPITCZ presents a second southern band in the eastern Pacific around 5°S from February to May (Huaman and Takahashi 2016, Huaman and Schumacher 2018). This

southern band of the East Pacific ITCZ explains the existence of more precipitation in the central and northern parts of the WCSA (north of 6°S) than in the southern WCSA because the dry effect of the meridional subsidence branch of the second band of the East Pacific ITCZ over this region (Takahashi and Martínez 2019). Regarding Central Pacific ITCZ (hereafter CPITCZ), Sulca *et al* (2018), who defined the ITCZC index, reported that positive ITCZC phase causes significant dry conditions over the northern Peruvian coast during DJF season due to the effect of the subsiding branch of the East Pacific ITCZ. Excluding strong El Niño events, Yu and Zhang (2018) found that precipitation over the northeastern equatorial Pacific is linearly correlated with local warm SST anomalies. In contrast, precipitation over the southern equatorial Pacific is not linearly correlated with local warm SST anomalies. The authors also noted that the nonlinear relationship precipitation-SST relationship over the southern equatorial Pacific is not driven by local SST anomalies. In addition, they stated that the interannual variability of local SSTs in the southern equatorial Pacific remains in phase with central Pacific SST anomlies. Moreover, Yu and Zhang (2018) found that the surface wind divergence field explains the spatial pattern and the SST-precipitation relationship across the equatorial Pacific Ocean during the austral fall (February-March-April) in weak El Niño years.

The precipitation in the northern Peruvian coast (NPC) exhibits a well-defined annual cycle, with wet months between December and April, whereas as dry season occurs from May and November, with the amount of the precipitation rising toward Ecuador (Rau *et al* 2017). NPC precipitation has a nonlinear relationship with SST associated with the activation of deep convection (Jauregui and Takahahsi 2018), which is occurs when SST exceeds a threshold value that along the coast of Peru is around 26 °C (Woodman 1998, Takahashi 2004). This nonlinear behavior also was observed between the February-April mean SST and Piura river discharge in northern Peru (Takahashi and Martínez 2019). Consequently, seasonal precipitation prediction poses significant challenges in the WCSA. This difficulty is largerly due to the limited number of meteorological stations with long-term precipitation records along the coasts of northern Peru and Ecuador. The limitation of the station network has been partly addressed through the recent development of various gridded precipitation products. These products are created by integrating data from rain-gauge stations with satellite precipitation data, such as the Peruvian Interpolated data of SENAMHI's Climatological and Hydrological Observations version 2.1 (PISCOpv2.1; Aybar *et al* 2020) and the Rain for Peru and Ecuador (RAIN4PE, Fernandez-Palomino *et al* 2021).

Another challenge stems from the scarcity of dynamic and statistical models capable of accurately predicting DJF precipitation anomalies in the WCSA (Gutierrez *et al* 2005, Bazo *et al* 2013, Recalde-Coronel *et al* 2014, De Guenni *et al* 2017, Vavrus *et al* 2022, SENAMHI 2023). The dynamical models largely corresponds to initialized global climate model (GCM) systems. Manzanas and Gutiérrez (2019) performed a process-conditioned bias-correction technique to 1- and 4-month lead to DJF precipitation in the northwestern part of Peru from the ECMWF System4 forecast model for the period 1981–2010. The bias-correction technique is based on an empirical-quantile mapping method which runs conditioned on the state of the Southern Oscillation Index (SOI, Trenberth 1984). Vavrus *et al* (2022) reported that the North American Multi-Model Ensemble (NMME; Kirtman *et al* 2014) predicts DJF precipitation anomalies over the northern Peruvian coast from 1982 to 2020. However, the authors did not provide a dynamic explanation for the successful performance of the ensemble of the coupled global climate models. The authors also pointed out that the Coupled Forecast System version 2 (CFSv2) model is the second out of the seven models of the NMME in present low bias for the DJF precipitation over northwestern Peru for forecast lead time. Ratterman *et al* (2023) reported that the CFSv2 seasonal prediction system has improved its ENSO prediction skill compared to the previous version. For example, Ratterman *et al* (2023) noted that the CFSv2 model shows a low bias in forecasting U.S. precipitation with lead times of 1 to 4 months. The CFSv2 model presents a significant correlation between observed and predicted precipitation anomalies over northwestern Peru in December and January of the following year, while the correlation is not statistically significant from February to May. The efficient prediction is due to the CFSv2 model replicating observed SST variability over the Niño 1 + 2 region in November and December. For the Ecuadorian coast, Recalde-Coronel *et al* (2014) reported that the ECHAM4.5 forecast has a lower precipitation prediction skill along the coast of Ecuador. This is attributed to the inadequacy of the constructed-analog statistical model in accurately predicting the SST Pacific Ocean to force ECHAM4.5.

Regarding statistical models, Bazo *et al* (2013) proposed exponential and linear models for the precipitation over northwestern Peru and found that the exponential model provides a substantially better results. The predictors for these statistical models included the average SST anomalies over the Indian Ocean, the Niño3.4 region, and the eastern tropical Atlantic Ocean. Regarding the Ecuadorian coast, Rossel and Cadier (2009) found that precipitation and meridional wind indices are better predictors than the Niño1 + 2 SST index to predict February and March rainfall in Guayaquil. De Guenni *et al* (2017) proposed a transfer function model based on the Niño3 index to predict monthly precipitation along the Ecuadorian coast several months in advance. However, this model was validated for the period 1982–2012, indicating that it did not consider the recent extreme El Niño episodes in DJF 2016, 2017, and 2023 in its validation. Petrova *et al* (2021) found that

the Niño3.4 index can be used to predict precipitation with 2-month lead the Ecuadorian coast. Thielen *et al* (2021) pointed out that entire North Atlantic SST anomalies are positively correlated with 3- and 4-month leads with precipitation of the Daule-Peripa reservoir (coast of Ecuador) for the period 1981–2017. Additionally, Rossel and Cadier (2009) documented that the meridional shift of the East Pacific Intertropical Convergence Zone is negatively correlated with DJF precipitation anomalies over the entire WCSA, even extending southward until the coast of central Peru (Sulca *et al* 2018). However, Rossel and Cadier (2009) utilize the meridional wind to predict the East Pacific ITCZ, while Sulca *et al* (2018) utilize a precipitation index. Despite the Pacific El Niño, Central and East Pacific ITCZ indices being significantly correlated with DJF precipitation across WCSA, they have not been utilized to forecast DJF precipitation anomalies in this region. In contrast, the Servicio Nacional Meteorológico e Hidrológico del Perú (SENAMHI) produces the official probabilistic austral summer precipitation forecasts the entire Peruvian territory divided into 13 broad regions, of which the northwestern coast is one, through empirical models that combine the outputs of dynamical models and station data using the Climate Predictability Tool (CPT) software from the International Research Institute for Climate and Society (IRI) (SENAMHI 2023).

According to current state-of-the-art statistical prediction models, the El Niño Pacific SST and ITCZ indices have not been utilized to construct a statistical prediction model for the DJF precipitation along the coasts of northern Peru and Ecuador. Therefore, this study aims to develop a statistical model to predict DJF precipitation with high spatial resolution using Pacific El Niño SST indices and East Pacific ITCZ indices, thus elucidating the significance of these predictors in forecasting. The primary advantage of the statistical prediction model lies in its computational efficiency, speed, and superior grid resolution compared to dynamic prediction models (Tran-Anh and Taniguchi 2018).

2. Data and methods

2.1. Data

We used monthly gridded sea surface temperature (SST) data called HadISST, constructed by the Met Office Hadley Centre (Rayner *et al* 2003). The horizontal grid resolution of the HadISST data is $1^\circ \times 1^\circ$, covering the period from 1870 to 2023.

We used monthly global gridded precipitation data from the Global Precipitation Climatology Project (GPCP, Adler *et al* 2003). The GPCP dataset has a horizontal resolution of $2.5^\circ \times 2.5^\circ$ and covers the period 1979–2024. For Peru, we utilized monthly high-resolution gridded precipitation data called Peruvian Interpolated data of SENAMHI's Climatological and Hydrological Observations version 2.1 (PISCOpv2.1, Aybar *et al* 2020), was used. The PISCOpv2.1 dataset was developed by the Servicio Nacional de Meteorología e Hidrología del Perú (SENAMHI). This dataset combines satellite precipitation products from the CHIRPS and precipitation station data. The data grid for PISCOpv2.1 is 10 km × 10 km, covering the period 1981–2023. It could be found at https://iridl.ldeo.columbia.edu/SOURCES/.SENAMHI/.HSR/.PISCO/.Prec/.v2p1/.unstable/.monthly/?Set-Language=es. The PISCOpv2.1 dataset is used to monitor drought and flood over the entire Peruvian territory (Llauca *et al* 2021).

This study used the monthly time series of the central and eastern Pacific El Niño SST indices (C and E; Takahashi *et al* 2011). The C and E indices are orthogonal and are calculated using SST data from the ERSSTv5 dataset. Essentially, it involves the rotation of the first two principal components of SST inside the belt of the equatorial Pacific Ocean (141° E-80° W, 5° S-5° N) by 45°. The monthly time series of the C and E indices cover the period from 1854 to the present and can be freely downloaded from the IGP website (https://met.igp.gob.pe/datos/ecindex_ersstv5.txt).

The indices for the meridional displacement of the Central and East Pacific Intertropical Convergence Zone (CPITCZ and EPITCZ) were computed as the first two rotated principal components of the monthly precipitation anomalies over the equatorial Pacific inside the box (131.25–88.75° W, 18.75°S-18.75° N, figure S1). We chose this specific region because it captures the two spatial patterns of the East Pacific ITCZ (Huaman and Schumacher 2018). The EPITCZ index was rescaled by a factor of −1 to establish that the East Pacific ITCZ is displaced toward the south, as in Sulca *et al* (2018).

2.2. Global climate model forecasts

In February 2021, a new version of the Geophysical Fluid Dynamics Laboratory (GFDL) model for Prediction and EArth System Research called the GFDL-SPEAR model (Zhao *et al* 2018a, 2018b, Delworth *et al* 2020) was made available as part of the NMME. Lu *et al* (2020) described the GFDL-SPEAR seasonal prediction system and its initialization procedure, and reported that it has improved ENSO prediction skill relative to previous systems. However, there is no study about the performance of the GFDL-SPEAR model to reproduce and predict DJF precipitation variability in the western coast of South America. Monthly SST and precipitation

datasets of the hindcast and forecast simulations from GFDL-SPEAR were used. These SST datasets from the GFDL-SPEAR model have a horizontal grid resolution of $1^\circ \times 1^\circ$ and cover the period January 1991-October 2024. The monthly hindcast data of SST and precipitation, consisting of 15 members (i.e., experiments), covers the period from Jan 1991 to December 2020. The monthly forecast data (predictions) cover the period from January 2021 to October 2024, consisting of 30 members. Both the monthly hindcast and forecast data include 12 leads.

Ensemble-mean monthly anomalies of SST and precipitation for the first 12 ensemble members from the GFDL-SPEAR model from January 1991 to October 2024 are calculated by removing their respective monthly climatology, obtained for each lead time separately, representing the average values from 1992 to 2017. Subsequently, the linear trend is removed from these monthly anomaly data for each lead time.

We consider DJF mean forecasts initialized on December 0.5 lead time. January and February data are taken from the 1.5 and 2.5 lead times, respectively. We removed the linear trend of DJF time series of the SST and precipitation anomalies. In addition, we tested whether the MLR model can predict DJF WCSA precipitation using SON data, despite the weak relationship between the average SON of the Pacific El Niño SST and the ITCZ indices and DJF WCSA precipitation.

The Central and Eastern Pacific El Niño SST (C and E) indices for GFDL-SPEAR are computed as the first two rotated principal component (RPC) of predicted monthly equatorial Pacific SST anomalies (141°E-80°W, 5°S-5°N) separately for each lead time. The CPITCZ and EPITCZ indices were calculated as for observations but using the forecasted anomalies.

2.3. The multiple linear regression (MLR) models

To estimate and predict standardized precipitation anomalies during DJF seasons along the coast of northern Peru and Ecuador, we developed statistical models using multiple linear regression (MLR) techniques considering i) observational versus GCM-predicted inputs (hereafter MLR_{OBS} and MLR_{PRED} model, respectively), and ii) regional-average versus grid point outputs. In addition, we applied K-mean clustering technique to identify regions within WCSA with similar intensity variability of the DJF standardized precipitation anomalies. We utilized the *kmeans* function in Matlab (Arthur and Vassilvitskii 2007). The six specific regions located within WCSA are labelled R1, R2, R3, R4, R5 and R6.

We used the multiple linear regression (MLR) model (DuMouchel and O'Brien 1989) based on iterative reweighted least squares (Beaton and Tukey 1974) as in Sulca *et al* (2021). The regional-average MLR models were built for six specific regions located within WCSA: R1, R2, R3, R4, R5 and R6. Our empirical–statistical model is based on the linear combination of the ENSO and ITCZ indices. The general equation of the MLR model is:

$$Y(t) = a_n X_n(t) + b + \varepsilon, \ldots \quad (1)$$

In this equation, Y(t) signifies the target or predictor variable (precipitation, PRE), varying with time t; $X_n(t)$ denotes the time series of the n-th predictor (Pacific El Niño SST and ITCZ indices); a_n and b are the least squares regression parameters (MLR slopes and intercept, respectively), and the repeated subindex n imply summation over n. These parameters are determined by minimizing the error ε. The MLR model was fitted using data for the period 1982–2011, while the data for the period 2012–2023 was reserved for validation. Predictors employed in the MLR model include E, C, CPITCZ, and EPITCZ. For the MLR models with grid point outputs, the model was fitted independently at each grid point using all predictors. The confidence of the model for each grid point was assessed using the F-test at a 95% confidence level for the validation period. The MLR model underwent calibration for the period 1982–2011 and validation for the period 2012–2023. To predict DJF precipitation anomalies along the coast of northern Peru and Ecuador, we first fitted the models using the observational data (MLR_{OBS}). We then replicated the MLR model with the same predictors from the forecasts by the GFDL-SPEAR model (MLR_{PRED}) using the regressed coefficients of the MLR_{OBS}. The MLR_{PRED} model aims to take advantage of the large-scale forecast capability of the GFDL-SPEAR model to predict austral summer precipitation anomalies in this region.

The MLR model will not use predictors based on Atlantic SST anomalies because the Atlantic Ocean SST are not good predictors for predicting the precipitation over the northern Peruvian coast (Lagos *et al* 2008, Rau *et al* 2017) and the Ecuadorian coast (Recalde-Coronel *et al* 2014, Ilbay-Yupa *et al* 2021). Falk and Miller (1992) emphasized that the MLR model should be constructed to avoid suppressor effects among predictors. The suppressor effect refers to a change in the sign of the correlation between precipitation and predictors, as well as in the sign of the regression coefficient in the MLR model. The suppressor effect can occur for three reasons: a) the correlation between precipitation and a predictor is close to zero, reflecting random fluctuation around zero, b) the suppressor effect arises when two or more predictors that contain the same information (collinearity), making them somewhat redundant. c) the third cause, known as 'real suppression', occurs when a key

predictor variable, essential for understanding the true relationship between latent predictors, suppresses the effect of another predictor.

Finally, we will use Pearson and Spearman correlation coefficients to quantify the linear and monotonic relationships between two variables - continuous or ordinal, respectively (De Guenni *et al* 2017, Akoglu 2018, Sulca *et al* 2018, Manzanas and Gutiérrez 2019). Previous studies have reported that the Pearson correlation coefficient is more effective for identifying atmospheric teleconnection, although its assumption of a Gaussian distribution makes it highly sensitive to extreme values (outliers) (Manzanas and Gutiérrez 2019). Manzanas and Gutiérrez (2019) reported a significant negative correlation between the SOI index and austral summer precipitation along the northern Peruvian coast for the period 1982–2010. In contrast, several studies have used Spearman correlation coefficient for validation purposes (De Guenni *et al* 2017, Manzanas and Gutiérrez 2019). The Spearman correlation coefficient quantifies the persistence the monotonic relationship between two variables. In other words, it captures the persistence of the sign of association between the observed and simulated time series. Manzanas and Gutiérrez (2019) applied the Spearman correlation coefficient to evaluate the performance of their seasonal forecasting model-based on process-conditioned bias correction-at rain-gauge stations across northern Peru, for leads of 1 and 4 months.

3. Results

3.1. Spatial variability of the austral summer precipitation of WCSA

The K-mean technique analysis applied to austral summer standardized precipitation anomalies across WCSA identified six regions, labelled 'R1', 'R2', 'R3', 'R4', 'R5' and 'R6' (figure 2). The Ecuadorian coast includes two regions (R1 and R2), while the northern Peruvian coast comprises four regions (R3 to R6). As shown in figure 2, regions R1 and R2 correspond to the western (Manabi, Santa Elena, Guayas, western Esmeralda) and eastern (eastern Esmeralda, Los Rios and northern Guayas) portions of the Ecuadorian coast, respectively. Region R3 covers the northernmost part of the northern Peruvian coast (Tumbes and Piura) and the southernmost Ecuadorian Andes (El Oro and western Loja), between 2.7°S and 6°S. Region R4 includes southwestern Piura and the northernmost part of Lambayeque between, 6.4°S and 4.6°S. Region R5 covers southern Lambayeque and northwestern La Libertad, extending from 7.8°S to 6.5°S. Finally, region R6 spans the central part of western La Libertad. However, the result from this region R6 should be interpreted with caution, as the average DJF precipitation anomalies are based on fewer than 15 grid points.

This study examines the influence of extreme El Niño episodes on WCSA precipitation from 1982 to 2023 by analysing the evolution of DJF standardized precipitation anomalies across six WCSA regions (figure 3). During the extraordinary 1982/83 El Niño, regions R1, R2 and R3 recorded DJF 1983 values above 2 (figures 3(a)–(c)), while regions R4, R5 and R6 recorded values of 1.4, 0.6 and −0.6, respectively (figures 3(d)–(f)). These results indicate a southward decrease in the precipitation signal associated with the extraordinary El Niño, which gradually weakens from the Ecuadorian coast to the southernmost part of the northern Peruvian coast. During the extraordinary 1982/83 El Niño, figures 3(a)–(e) show that regions R1 to R5 recorded DJF anomaly values around 5, while R6 recorded a value of 2.2 (figure 3(f)). These results suggest that the 1997/98 El Niño had a stronger influence on WCSA precipitation that the 1982/83 event. In contrast, during DJF 2022/23, region R6 recorded a value of 2 (figure 3(f)), while regions R1 to R5 recorded values ranging from zero to negative (figures 3(a)–(e)). Therefore, DJF precipitation in region R6 appears to be less responsive to El Niño conditions than in the other regions (R1 to R5). This is consistent with the absence of a significant positive correlation between the DJF SST anomalies in the eastern Pacific and DJF precipitation anomalies over region R6 (figure 4(f)). The weak response of DJF precipitation in region R6 is also consistent with a ~11-year decadal signal (figure 3(f)). This decadal precipitation signal over central La Libertad was previously reported by Bourrel *et al* (2014). Another possible factor is the limited number of grid points used to calculate the average DJF precipitation anomalies in region R6.

3.2. Impact of the ENSO Pacific SST and the ITCZ indices on austral summer precipitation over South America

This study examines the impact of El Niño Pacific SST and ITCZ indices with DJF precipitation over South America from 1982 to 2023, using spatial, linear regression patterns derived from the GPCP precipitation dataset (figure 5). Figure 5(a) shows that warm phase of the Eastern Pacific El Niño SST (E) index is associated with wet anomalies across the equatorial Pacific (10°S-5°N), although the intensity of these anomalies decreases from the western Pacific toward the northern Peruvian coast. It also is associated with enhance DJF precipitation anomalies across the northern Peruvian Andes. The warm phase of the Central El Niño Pacific SST (C) index (figure 5(b)) is associated with wet anomalies across the equatorial Pacific (7°S-5°N), although their intensity decreases from the western Pacific toward the northern Peruvian coast. In addition, it is

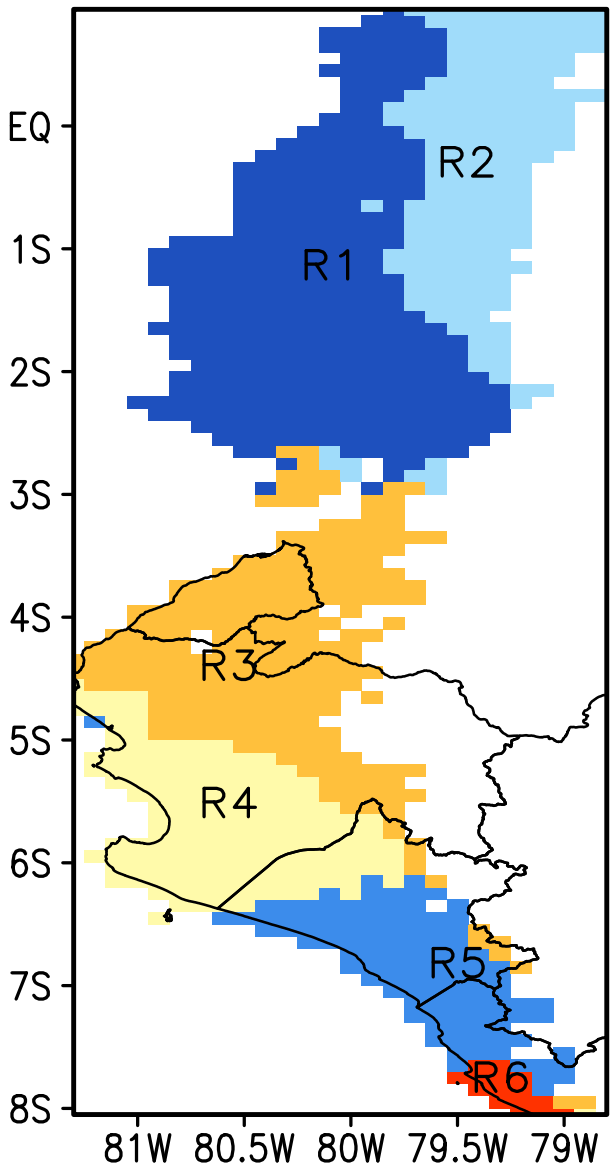

Figure 2. The locations of six specific areas of western coast of South America (WCSA) for topographic elevations below 1000 m asl are shown in shading: the region R1 (purple), the region R2 (sky blue), the region R3 (orange), the region R4 (yellow), the region R5 (blue) and the region R6 (red). Monthly PISCOpv2.1 dataset was used in this analysis.

associated with a northeast-southwest precipitation dipole over the southwestern Pacific, linked to an enhanced South Pacific convergence zone (SPCZ). Conversely, it also leads to reduced DJF precipitation over the northern coast and Andes of Peru. This precipitation reduction is linked to an enhanced subsidence branch of the Pacific Walke cell during Central Pacific El Niño events (Sulca 2021) and the equatorial propagation of upper-level Rossby wave trains triggered by the intensified SPCZ (Van der Wiel *et al* 2016).

The positive phase of the Central Pacific ITCZ (CPITCZ) index (figure 5(c)) is associated with wet anomalies over the western Pacific and along the equatorial band (1°N-10°N), although the intensity decreases from the western Pacific toward the northern Peruvian coast. In addition, it is less associated with the edge of the SPCZ compared to the ITCZC index proposed by Sulca *et al* (2018). It highlights that positive ITCZC index is a linear response to warm SST anomalies over the western Pacific Ocean. These results show that the CPITCZ index more effectively captures precipitation teleconnections associated with the central Pacific ITCZ than the ITCZC index. In addition, the positive CPITCZ index is associated with reduced DJF precipitation along the northern Peruvian coast, likely due to the descending branch of the deep convection linked to the warm SST anomalies over western Pacific Ocean (Bayr *et al* 2014). In contrast, the positive phase of the East Pacific ITCZ (EPITCZ) index (figure 5(d)) is associated with wet anomalies across the equatorial Pacific (13°S-0°N), with greater intensities from the western Pacific to the northern Peruvian coast than during warm E index

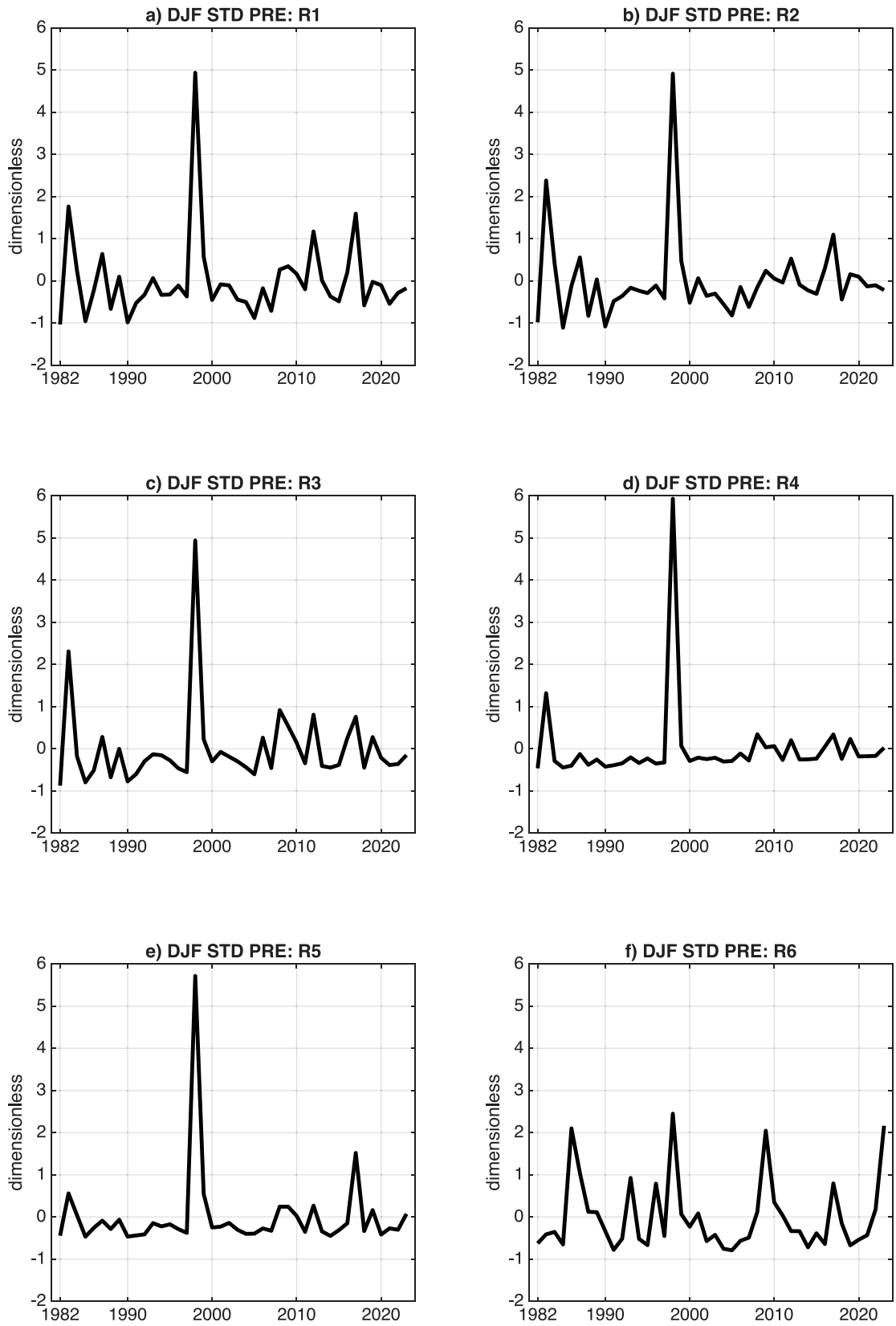

Figure 3. Time series of the average DJF standardized precipitation anomalies of all grid points within the six specific areas of western coast of South America (WCSA) for the period 1982–2023: (a) the region R1, (b) the region R2, (c) the region R3, (d) the region R4, (e) the region R5, and (f) the region R6. Monthly PISCOpv21 dataset was used in this analysis.

(figure 5(a)). These wet anomalies over the far-eastern Pacific are a response to the southward shift of the east Pacific ITCZ (Huaman and Schumacher 2018). In addition, positive EPITCZ index is linked to increased DJF precipitation over the northern Peruvian Andes, while much of the rest of Peru experiences dry anomalies.

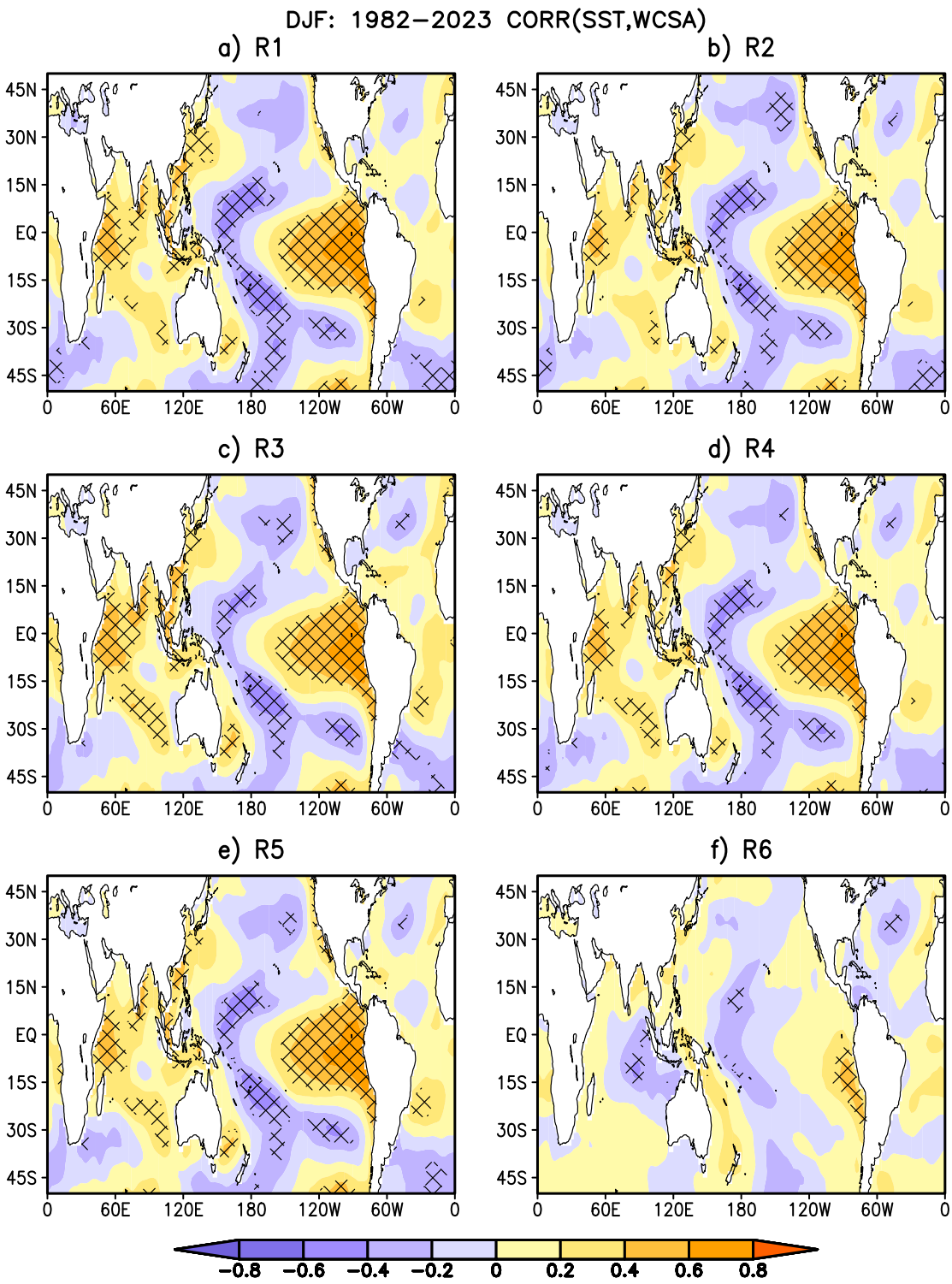

Figure 4. Spatial correlation of DJF global sea surface temperature anomalies (SST, °C) with (a) the region R1, (b) the region R2, (c) the region R3, (d) the region R4, (e) the region R5, and (f) the region R6. Hatching represents a statistically significant correlation at the 95% confidence level. The analysis is based on austral summer (December–January–February, DJF) averages for the 1982–2023 period. Monthly HadISST dataset was used in this analysis.

3.3. Relationship between the WCSA precipitation and the observational ENSO and ITCZ indices

Precipitation over Ecuadorian Andes positively correlates with the Niño3 index from October to November (figures 6(a)–(b)). In contrast, northern and southern portions of the northern Peruvian coast are not correlated with the Niño3 index in November (figures 6(a), (b)). This finding is consistent with the moderately positive correlation between the Niño3 index and monthly precipitation along the Ecuadorian coast from 1982 to 2012 (De Guenni *et al* 2017). Precipitation over most WCSA positively correlates with the Niño3 index from December to February of the following year, but the correlation coefficients are weaker than 0.8 (figures 6(c)–(e)).

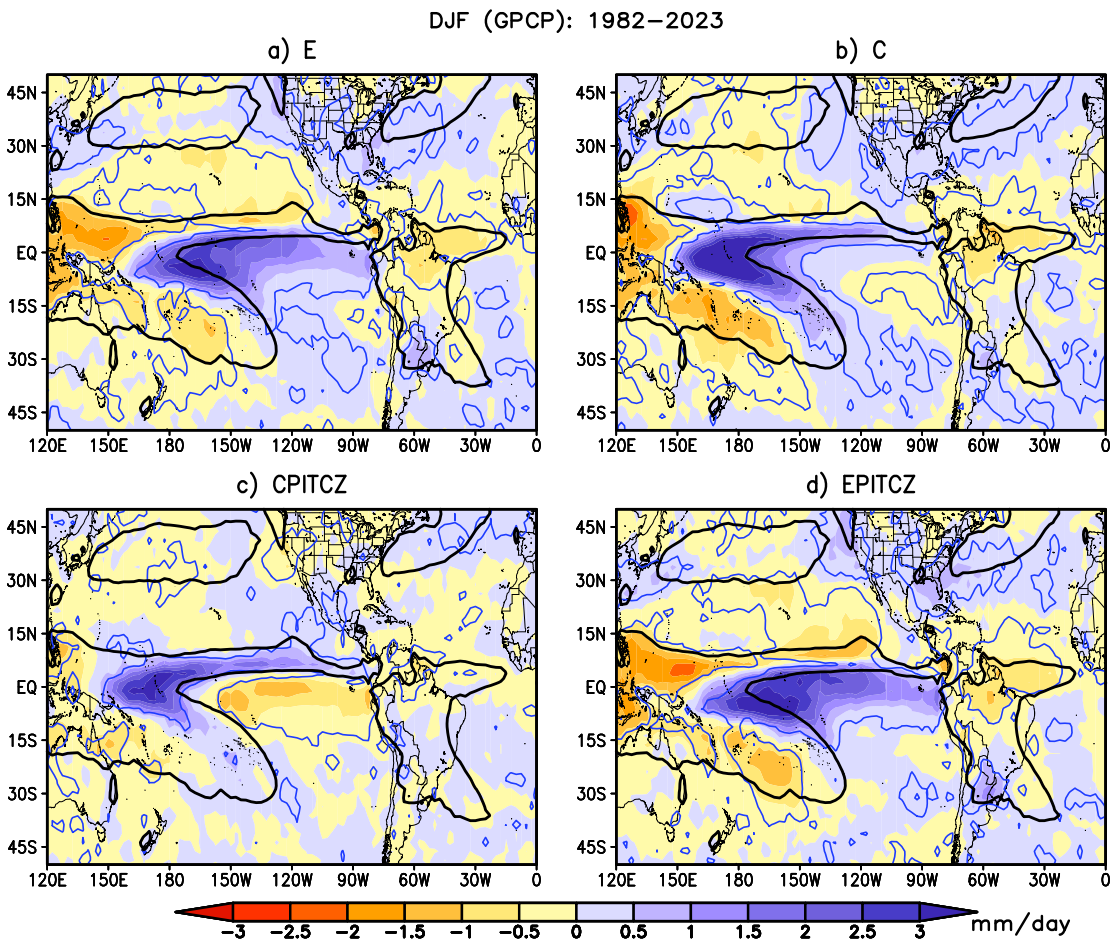

Figure 5. Linear regression coefficients between DJF GPCP precipitation and (a) the Eastern Pacific El Niño SST (E) index, (b) the Central Pacific El Niño SST (C) index, (c) the Central Pacific Intertropical Convergence Zone (CPITCZ) index, and (d) the East Pacific Intertropical Convergence Zone (EPITCZ) index. Values are in mmday^{-1} for one standard deviation of each corresponding ENSO and ITCZ indices. Blue (Red) shading represents positive (negative) precipitation anomalies in intervals of 0.5 (−0.5) mm day^{-1} per standard deviation. Black contour represents the climatological isoline of 4 mm day^{-1}. Blue contours represent significant correlation between Pacific El Niño SST and ITCZ indices and precipitation at the 95% confidence level. Analysis based on the period 1982–2023.

Figures 6(f)–(j) show that the E index resembles monthly spatial correlation related to the Niño3 index, but they are stronger ($r > 0.8$, $p < 0.05$). This finding reveals that the E index would be used solely to build season-ahead regression models for the Ecuadorian coast. In contrast, the C index shows no significant correlation with monthly precipitation along the coast of northern Peru and Ecuador (figures 6(k)–(n)).

Concerning the Central Pacific Intertropical Convergence Zone (CPITCZ) index, the sign of spatial precipitation correlation varies from weakly positive in October, particularly over the southern part of the northern Peruvian coast and central and northern parts of the Ecuadorian coast, to substantially negative in January and February (figures 6(p)–(t)). The correlations turn negative starting from December (figures 6(r)–(t)) but are strong and statistically significant in January and February (figures 6(s), (t)). These findings show that the CPITCZ index has a negative linear relationship with DJF precipitation over the western coast of South America. In contrast, as expected, the eastern Pacific ITCZ (EPITCZ) index, strongly and positively correlates with monthly precipitation over the WCSA from October to February of the following year, except for the northern Peruvian coast in October (figures 6(u)–(y)). Figures 6(v)–(y) also show that these positive correlations are stronger than in the N3 and E indices (figures 6(b)–(e) and (g)–(j)). Despite the maximum values of the E and EPITCZ indices coinciding during extraordinary El Niño events, they are associated with different DJF precipitation and lower- and upper-level atmospheric circulation patterns over South America (Sulca *et al* 2018), indicating that these two large-scale forcings have different interannual variability. Also, the EPITCZ index can be expected to perform better than others because it is based on precipitation anomalies and should be therefore linearly related to the WCSA precipitation, while the indices based on SST anomalies are known *a priori* to be nonlinearly related with precipitation (Woodman 1997, 1998, Takahashi and Dewitte 2016, Sulca 2021). Thus, the EPITCZ index emerges as the best predictor for monthly precipitation in WCSA because it exhibits a positive linear correlation over most WCSA that is stronger than for the N3 and E indices.

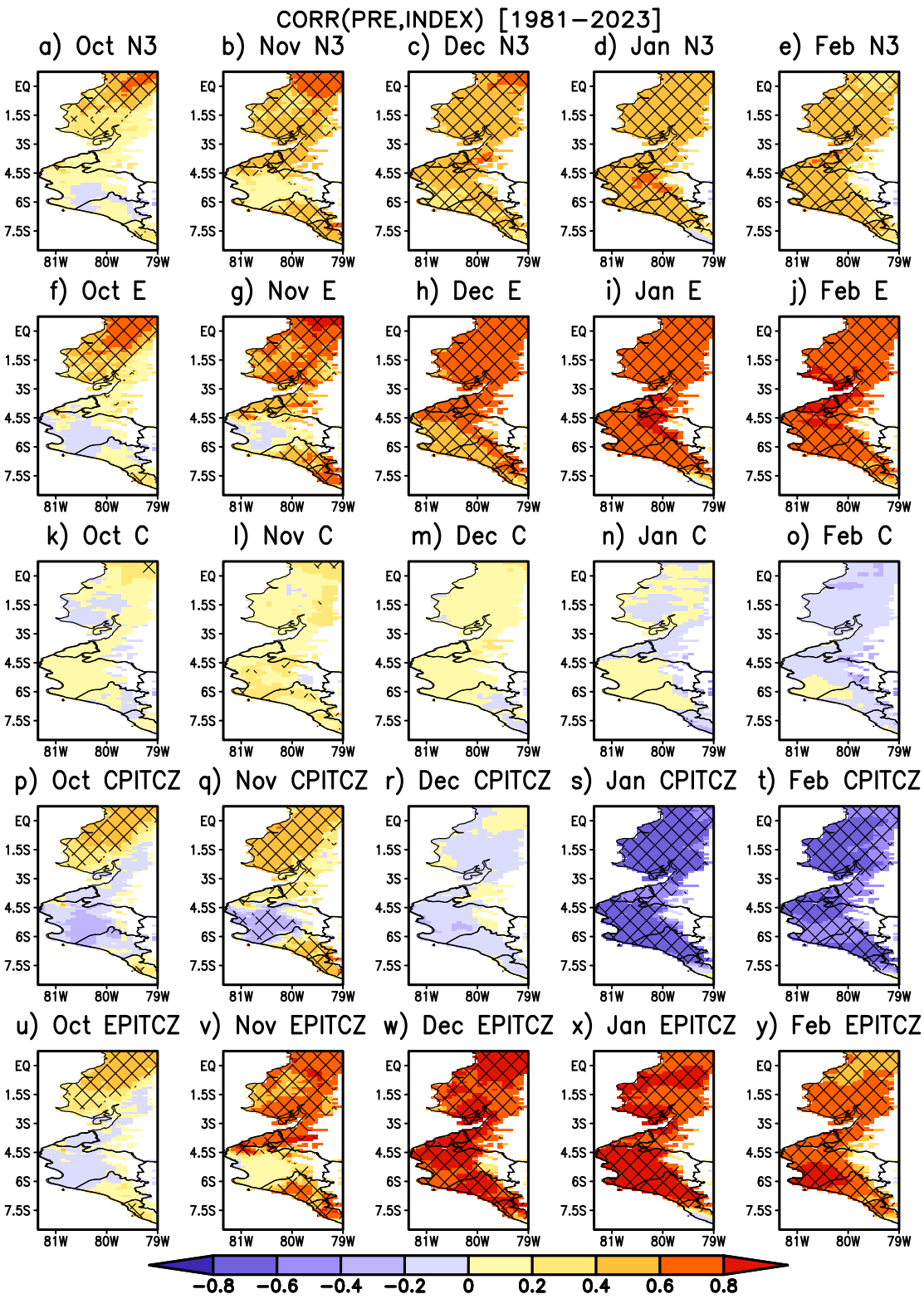

Figure 6. Spatial simultaneous correlation between monthly precipitation anomalies and the Niño 3 index over the western coast of South America (8.5°S-0.75°N) for the period 1981–2023 for topographic elevations below 1,500 m asl. during (a) October, (b) November, **c**) December, (d) January, and (e) February month. Hatching areas represent correlations statistically significant at the 95% confidence level. (f)–(j) As in (a)–(e), but for the Eastern Pacific El Niño SST (E) index. (k)–(n) As in (a)–(e), but for the Central Pacific El Niño SST (C) index. (p)–(t) As in (a)–(e), but for the Central Pacific Intertropical Convergence Zone (CPITCZ) index. (u)–(y) As in (a)–(e), but for the East Pacific Intertropical Convergence Zone (EPITCZ) index. The PISCOpv2.1 dataset was used in this analysis.

3.4. Validation of the ENSO and ITCZ indices from the GFDL-SPEAR model

Figure 7 displays the observed and predicted DJF time series of the ENSO and ITCZ indices from the GFDL-SPEAR model from 1992 to 2023. For the Pacific El Niño SST indices, the observed and predicted DJF time

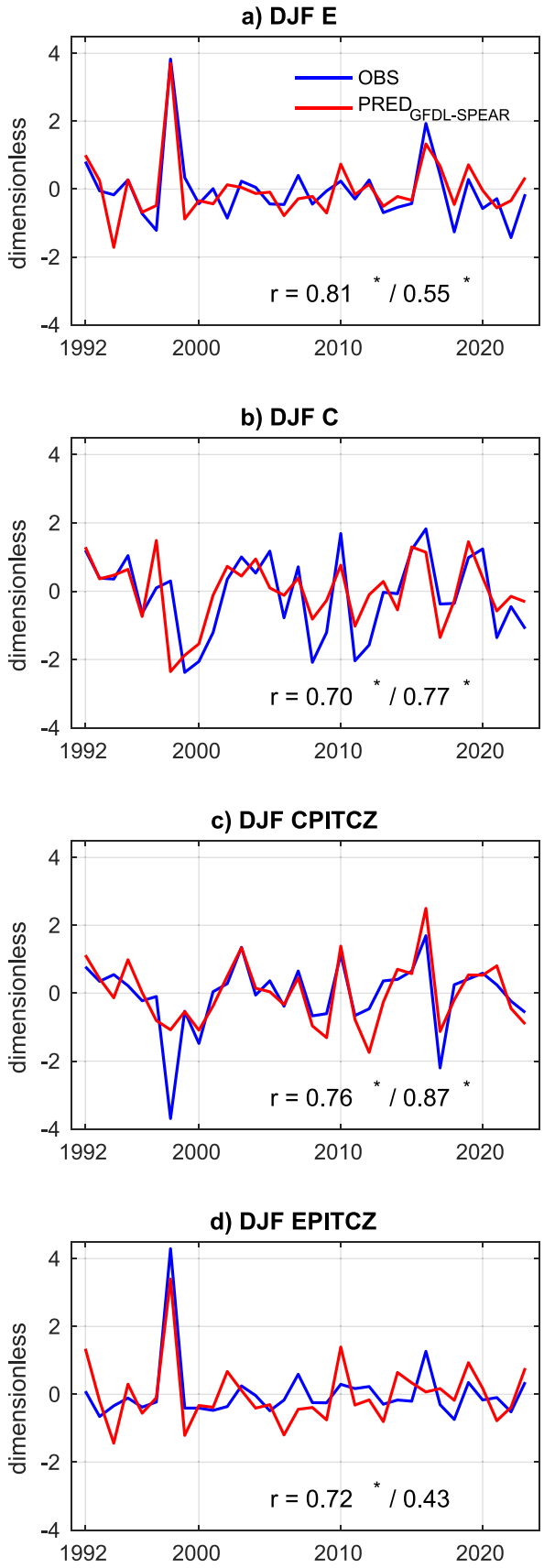

Figure 7. The observed (blue line) and predicted DJF time series by the GFDL-SPEAR model initialized in December (red line) for (a) the Eastern Pacific El Niño SST (E) index, (b) the Central Pacific El Niño SST (C) index, (c) the Central Pacific Intertropical Convergence Zone (CPITCZ) index, and (d) the East Pacific Intertropical Convergence Zone (EPITCZ) index. The black numbers represent the Pearson and Spearman correlation between observed and predicted by the GFDL-SPEAR model in the period 1992–2023. The black asterisk indicates statistically significant correlations at 95% confidence levels.

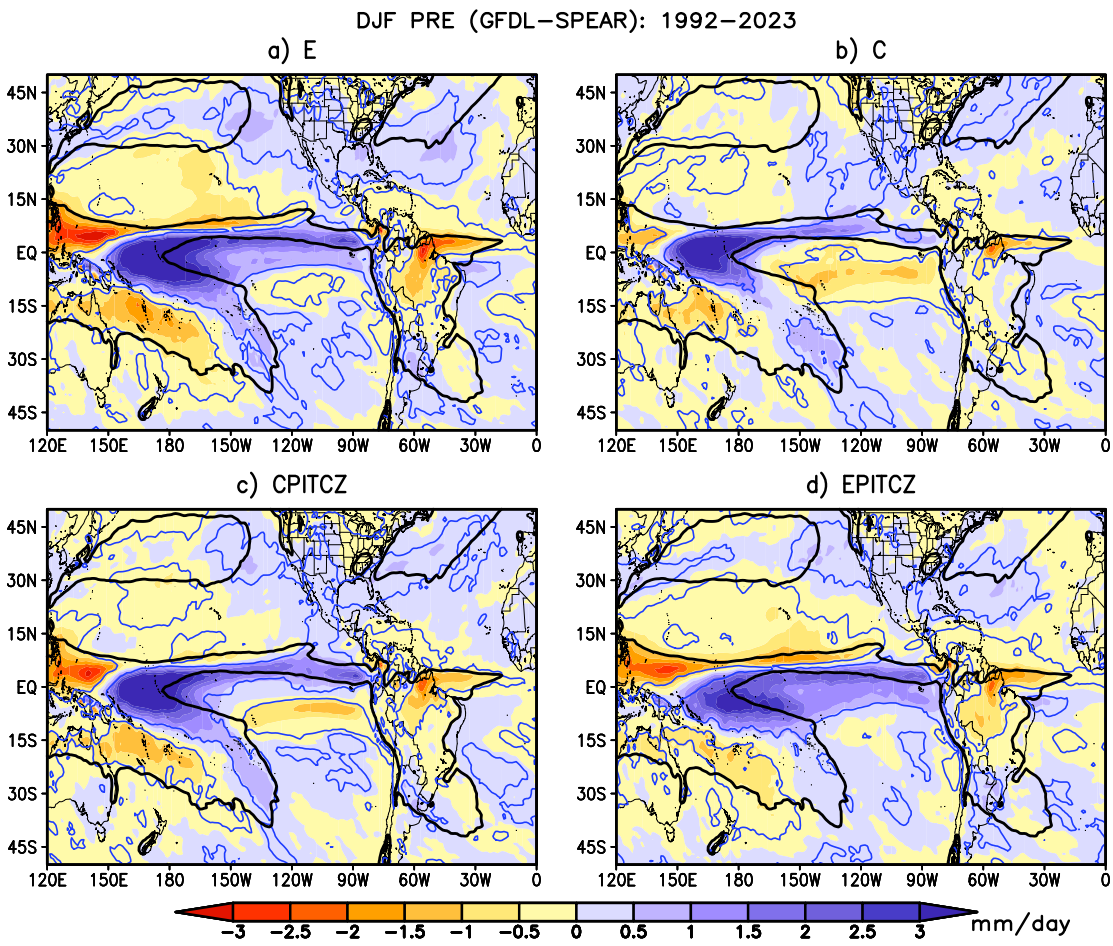

Figure 8. Regression of several indices upon DJF GFDL-SPEAR precipitation anomalies for (a) the Eastern Pacific El Niño SST (E) index, (b) the Central Pacific El Niño SST (C) index, (c) the Central Pacific ITCZ (CPITCZ) index, and (d) the East Pacific ITCZ (EPITCZ) index. Scale for precipitation anomalies (in mm day^{-1} per standard deviation). Blue contours represent significant correlation between both Pacific El Niño SST and ITCZ indices and precipitation at the 95% confidence level. Red (blue) shading represents positive (negative) precipitation anomalies. Contour interval is 0.5 mm day^{-1} per standard deviation. Black contour represents the climatological isoline of 4 mm day^{-1}. Analysis based on the period 1992–2022.

series of the E and C indices show positive correlations throughout the period from 1992 to 2023, with correlation coefficients of Pearson 0.81 and 0.70, respectively (figures 7(a), (b)). However, the E index presents a lower Spearman correlation of 0.55, as the good predictions of the large El Niño events of 1998 and 2016 increase the Pearson correlation, but the lower performance in predicting the weaker variability is penalized by the Spearman coefficient (figure 7(a)). In fact, if we remove 1998 and 2016, the Pearson correlation decreases to 0.43. The lower skill for the eastern Pacific than for the central Pacific is a general feature of global climate forecast model systems (Ding *et al* 2020; Rivera-Tello *et al* 2023). This is possibly due to the generalized warm and wet biases in the eastern Pacific in the climate models and the importance of nonlinear ocean-atmosphere El Niño processes in this region, particularly the existence of a threshold in SST for deep atmospheric convection (e.g. Takahashi and Dewitte 2016, Ding *et al* 2018, Srinivas *et al* 2024). In contrast, the GFDL-SPEAR model accurately predicted the sign of the C index, with both correlation coefficients above 0.7, but sometimes it misrepresented the strength (figure 7(b)). The underestimation by part of the predicted C index is explained by the inability of the GFDL-SPEAR model to simulate the positive feedback associated with enhanced SPCZ observed during warm C index (figure 8(b)).

Regarding the ITCZ indices, the observed and predicted DJF time series of the CPITCZ indices have high correlation, with Pearson and Spearman coefficients of 0.76 and 0.87, respectively (figures 7(c)–(d)). However, the GFDL-SPEAR model strongly underestimated the large negative value during the extreme El Niño in 1998. Although the predicted CPITCZ index reproduces the observed precipitation pattern (figure 8(c)), the underestimation of the 1998 anomaly likely results from deficiencies in the GFDL-SPEAR model in the simulation of the enhanced SPCZ associated with the Central Pacific El Niño SST (C) index (figure 8(b)) because the GFDL-SPEAR model simulated accurately the E and EPITCZ indices (figures 8(a), (c)). On the other hand, the variability of the EPITCZ index is only moderately well reproduced (figure 7(d)), except for the large El Niño value in 1998, which is reflected by the low (and non-significant) Spearman (0.43) relative to the Pearson coefficient

(0.72). Some predictions even had the opposite sign to the observed, particularly before 2017 (figure 7(d)). The limited skill in predicting the EPITCZ index may be attributed to an overestimation of the intensity of the positive feedback between warm SST anomalies over eastern Pacific basin and precipitation across the entire ITCZ, which inducing wet anomalies along the Peruvian coast (figure 8(d)), rather than being confined to the northern Peruvian coast as observed pattern (figure 5(d)).

3.5. Performance of the MLR model

The MLR_{OBS} model accurately reproduces the interannual variability of DJF precipitation anomalies over the northern Peruvian Andes and the Ecuadorian coast using the PISCOpv2.1 dataset, as indicated by significant positive correlations greater than 0.6 observed in all these regions, with the highest correlations found in the southernmost part of the northern Peruvian coast (south of 6.5°S) and the northern Ecuadorian coast (north of 1°S) using the independent testing data for 2012–2023 (figure 9(a)). Figure 9(b) shows that the root mean square error ($RMSE_{OBS}$) presents the lowest values found along most of the northern Peruvian coast (< 10 mm month^{-1}), while the highest RMSE values are observed along the coast of Ecuador and the Peru-Ecuador border, ranging from 20 mm month^{-1} to 60 mm month^{-1}. The lowest RMSE values are consistent with previous studies that have reported a strong positive linear relationship between DJF precipitation in this region and the SST anomalies along the coast of northern Peru (Woodman 1998, Takahashi 2004) and the southern shift of the central and eastern Pacific ITCZ (Sulca *et al* 2018). The highest RMSE would be associated with the bias of PISCOpv2.1 dataset ranging from 60 mm month^{-1} to 160 mm month^{-1} caused by the lack of rain-gauge stations in these areas.

Figure 10 presents the spatial distribution of the slopes of the predictors (e.g., regressed coefficients) of the MLR_{OBS} model at each grid point along the western coast of South America. Figure 10(a) illustrates that the slope associated with the E index (a_E) has positive regression coefficients across Ecuadorian coast and northern NPC, with the strongest values (> 40 mm month^{-1}) over the southernmost and northeastern regions of the Ecuadorian coast. Conversely, the slope a_E shows negative regression coefficients between 0 and -20-mm month^{-1} across central and southern parts of the northern Peruvian coast, south of 5.2°S, but are not statistically significant. These results indicate that the E index has a suppression effect over central and southern parts of the northern Peru and Ecuador.

Figure 10(b) shows that the slope for the C index (a_C) exhibits positive and negative regression coefficients over the WCSA, but are not statistically significant, consistent in part with the negative correlation between WCSA precipitation and the C index (figures 6(k)–(n)). The slope for the CITCZ index (a_{CPITCZ}) has negative regression coefficients across the entire WCSA, consistent with the negative linear relationship between WCSA precipitation and the CPITCZ index in the austral summer months (December, January and February) (figures 6(r)–(t)). Conversely, the slope for the EPITCZ index (a_{EPITCZ}) has positive regression coefficients across the entire WCSA, which are twice larger as those for a_E. The predominance of positive regression coefficients aligns with the positive linear relationship between WCSA precipitation and the EPITCZ index (figures 6(u)–(y)). The positive values of the slope a_{EPITCZ} explains the suppression effect on the spatial pattern of a_E, as the strong correlation between the E and EPITCZ indices renders the E index redundant in certain regions of WCSA. These findings suggest that the ITCZ indices (CPITCZ and EPITCZ) are the two best predictors for estimating and forecasting DJF precipitation anomalies across most of WCSA via a statistical downscaling model.

We replicated the MLR_{OBS} model for DJF standardized precipitation anomalies over WCSA using predicted Pacific El Niño and ITCZ indices for the period 1992–2023 (hereafter MLR_{PRED}; figure 11). The MLR_{PRED} model accurately reproduces the interannual variability of DJF precipitation anomalies over the northern region of northern Peruvian Andes (north of 5°S) and the Ecuadorian coast, based on the PISCOpv2.1 dataset. Significant positive correlations (> 0.6) were observed in all these regions, using the independent testing data for 2012–2023 (figure 11(a)). The root mean square error ($RMSE_{PRED}$) presents the lowest values along the northern Peruvian coast (north of 5°S) and the Ecuadorian coast (< 1 STD) (figure 11(b)), while the highest RMSE values occur over the central and south parts of the northern Peruvian coast, ranging from 1.2 to 3 standard deviations.

The low RMSE values are consistent with the strong linear relationship between DJF precipitation in these regions and the SST anomalies along the coast of northern Peru and Ecuador (Woodman 1998, Takahashi 2004, Bazo *et al* 2013, De Guenni *et al* 2017), as well as with the southern shift of the central and eastern Pacific ITCZ (Rossel and Cadier 2009, Sulca *et al* 2018). The good performance of the MLR_{PRED} model suggests in regions R1, R2 and R3 indicates that the predicted E, CPITCZ and EPITCZ indices by the GFDL-SPEAR model can be utilized to forecast DJF precipitation over the northern Peruvian coast (north of 5°S) and Ecuadorian coast. In contrast, the highest RMSE values in regions R4 to R6 are primarily due to biases introduced by the very low accumulated DJF precipitation in these desert areas (Rau *et al* 2017), which hinders accurate

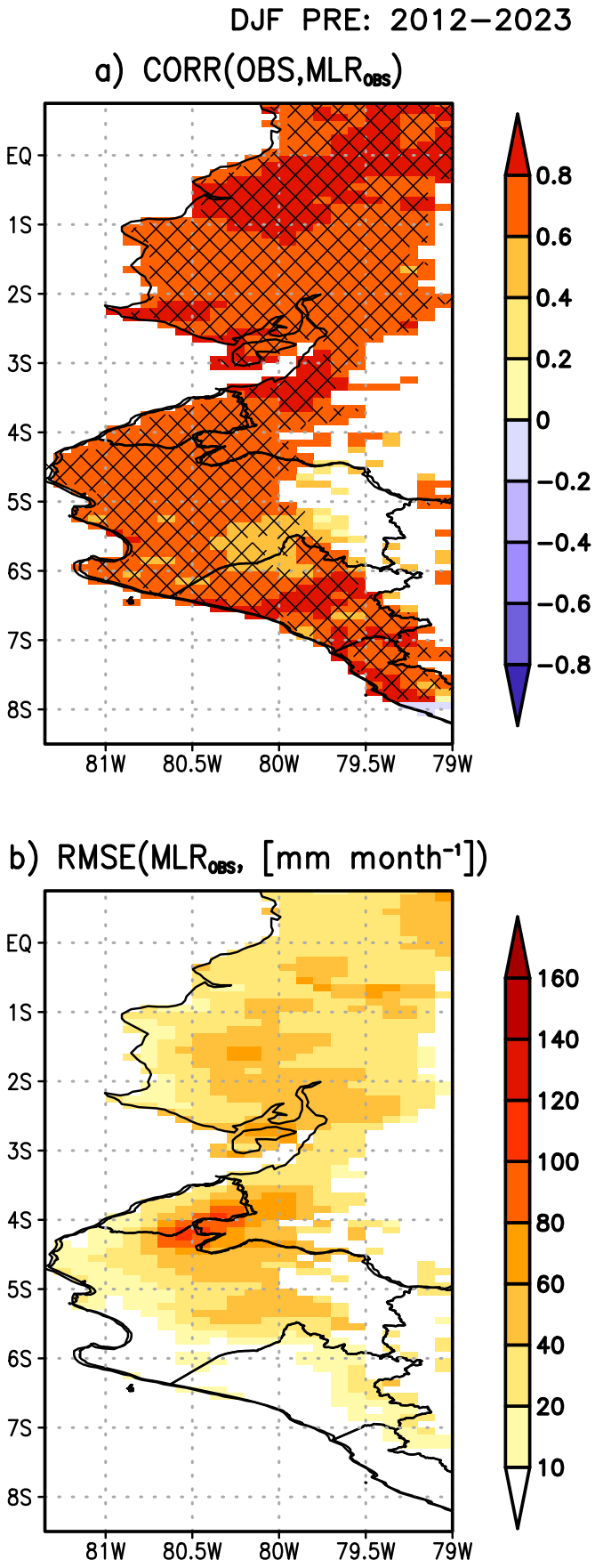

Figure 9. (a) Spatial correlation between the DJF precipitation anomalies in the western coast of South America (WCSA) for topographic elevations below 1,500 m asl. by the multiple linear regression (MLR_{OBS}) model during the austral summer seasons (December-January-February, DJF) in the validation period 2012–2023. Crossed-out regions indicate statistically significant correlations at the 95% confidence level. (b) The values of the root-mean-square error (RMSE) of the estimated precipitation for the MLR_{OBS} model. The PISCOpv2.1 product was used in this analysis.

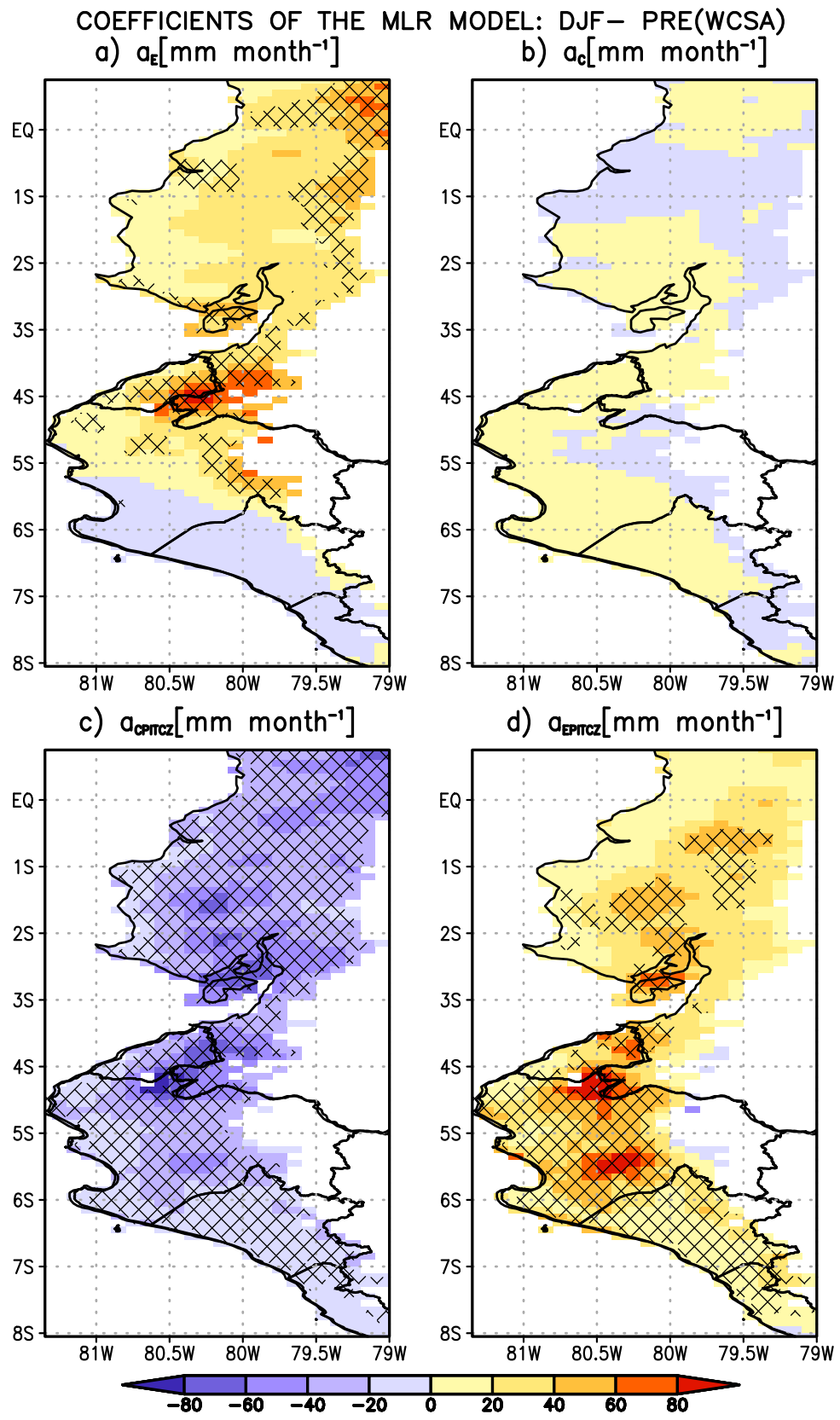

Figure 10. The spatial pattern of the slope of the predictors of the MLR_{OBS} model for each grid within western coast South America for topographic elevations below 1000 m asl.: (a) the Eastern Pacific El Niño SST (a_E) index, (b) the Central Pacific El Niño SST (a_C) index, (c) the Central Pacific ITCZ (a_{CPITCZ}) index, and (d) the East Pacific ITCZ (a_{EPITCZ}) index. The calibration period of the MLR_{OBS} model is 1982–2011. Crossed-out regions indicate statistically significant correlations at the 95% confidence level. The validation period is 2012–2023. The PISCOpv2.1 dataset was used in this analysis.

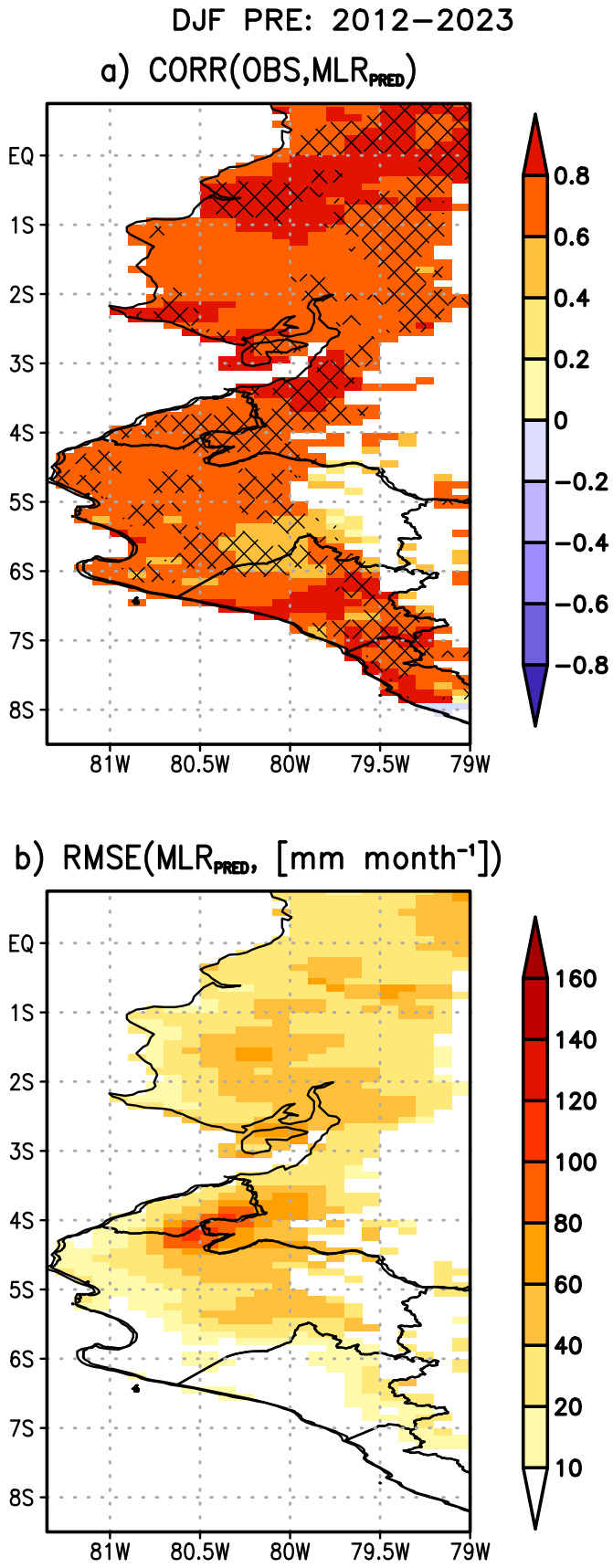

Figure 11. (a) Spatial correlation between observed and predicted DJF precipitation anomalies, which was initialized in December, across the western coast of South America (WCSA) for topographic elevations below 1000 m asl. by the multiple linear regression (MLR_{PRED}) model during the austral summer season (December-January-February, DJF) in the validation period 2012–2023. The MLR_{PRED} model is based on the regressed coefficients (e.g., slope) of the MLR_{OBS} model. Crossed-out regions indicate statistically significant correlations at the 95% confidence level. (b) The values of the root-mean-square error (RMSE) of the estimated precipitation for the MLR_{PRED} model. The PISCOpv2.1 product was used in this analysis.

standardization. This issue is further exacerbated by the limited availability of rain-gauge stations in the region (Aybar *et al* 2020).Therefore, the predictability offered by the MLR model for estimating and predict standardized precipitation anomalies over central and southern portions of the northern Peruvian coast in regions R4 to R6 —where bias values and decadal signal are high—should be considered with caution.

We replicated the MLR_{OBS} model for DJF standardized precipitation anomalies in six regions located within WCSA for the period 1982–2023 (figure 12). The equations and their respective Pearson correlations of the six MLR models are shown in table 1. We can see the none of the models considers C as a predictor, which could be expected, given their low correlations reported above, while E is a predictor for most of the regions except R6, with positive regression coefficients. On the other hand, the two Pacific ITCZ indices are considered predictors in all of the models, with negative coefficients in the case of CPITCZ and positive coefficients in the case of EPITCZ, with the latter being substantially larger than the coefficients for the E index.

During the DJF season, the MLR_{OBS} model reproduces the interannual variability of DJF standardized precipitation in all six regions within the WCSA, as the observed and estimated DJF seasons show a strong Pearson and Spearman correlation coefficients ($r \geqslant 0.55$, $p < 0.05$) (figures 12(a)–(f)). However, the MLR_{OBS} model shows a notable bias, tending to overestimate precipitation by −0.5 to 1 STD, while it underestimates precipitation across WCSA, except region R2 (western Ecuadorian coast), above 1 STD (figure 13). The underestimation in specific years highlights the need of atmospheric forcings of moisture advection and divergence to estimate austral summer WCSA precipitation as was hypothesized by De Guenni *et al* (2017). Table 1 shows that DJF WCSA precipitation is modelled by a linear combination of the E index and the ITCZ (CPITCZ and EPITCZ) indices. This indicates that DJF WCSA precipitation responds to deep convection caused by warm SST anomalies in the eastern Pacific Ocean and the southward shift of the central and/or eastern parts of the Pacific ITCZ. While the East Pacific ITCZ plays a significant role in DJF precipitation over WCSA, its influence is secondary to that of the E index.

DJF WCSA precipitation has high sensitivity to the diversity of El Niño events, with eastern and central Pacific warming or ITCZ enhancement produce opposing effects (Sulca *et al* 2018). However, climate forecast models can only distinguish E and C events in boreal winter skillfully with very short lead times, on the order of one month (Ren *et al* 2019). To assess predictability, we replicated the MLR model to predict DJF WCSA precipitation at a 3-month lead using the current (zero lead) Pacific El Niño SST and ITCZ indices, but the model showed very limited skill (not shown). These results indicate that the values of these indices during austral spring (September–October–November, SON) seasons are insufficient to predict the evolution of the large-scale climate system that is relevant for austral summertime precipitation in WCSA.

Additionally, we applied the MLR model for the six regions located within WCSA using the predicted E, CPITCZ and EPITCZ indices from the GFDL-SPEAR model with the regression coefficients of MLR_{OBS} (hereafter MLR_{PRED}; table 1). Table 1 illustrates that the MLR_{PRED} model accurately predicts DJF standardized precipitation anomalies for four out six regions within WCSA (R1, R2 and R6) exhibit strong positive Pearson correlations ($r > 0.72$, $p < 0.05$), except for regions R4, R5 and R6, which show a correlation below 0.49. In contrast, all six WCSA regions exhibit non-significant Spearman correlations (table 1), suggesting that the MLR_{PRED} model does not reliably capture the rank-based variability in precipitation, specially under ENSO-neutral conditions. These findings indicate that the GFDL-SPEAR model can predict DJF precipitation variability in the half of WCSA (R1, R2 and R3), except in the southern and central portions of the northern Peruvian coast (e.g., the regions R4, R5 and R6) (figure 11). When comparing the correlation coefficients and RMSEs of the MLR_{OBS} and MLR_{PRED} in table 1, most correlation coefficients and the RMSEs of the MLR_{OBS} are closer than those of the MLR_{PRED}, indicating than the GFDL-SPEAR model can provide accurate MLR models for the DJF anomaly values of the WCSA precipitation than the observed time series in the southern and central parts of the northern Peruvian coast. This is because the E and EPITCZ indices from the GFDL-SPEAR model includes noise from the unrealistic SPCZ teleconnection as well as overestimation precipitation teleconnections over Peru, unlike those in the observations. Moreover, this limitation could be due to the inefficiency of the GFDL-SPEAR model in simulating the remote influence of the C index on wind divergence over the eastern Pacific Ocean, which plays a key role in establishing the precipitation asymmetry linked to southward shifts in the position of the Eastern Pacific ITCZ (Yu and Zhang 2018).

4. Discussion and conclusions

Predicting austral summer precipitation along the coasts of northern Peru and Ecuador is challenging. Extreme precipitation tends to occur during El Niño events that feature high SST near the coasts (Takahashi 2004). However, even though several global climate models (GCMs) GCMs simulate the dynamics associated with strong eastern Pacific El Niño, they misrepresent the spatial patterns (Takahashi and Dewitte 2016, Cai *et al* 2018), which are important to determine the coastal impacts. This is most likely associated strongly with the large mean climatological biases in the southeast Pacific that persist in the GCMs, with strong positive SST and biases along the coast of Peru and Ecuador (Zhou *et al* 2020). Hence, the building of statistical downscaling

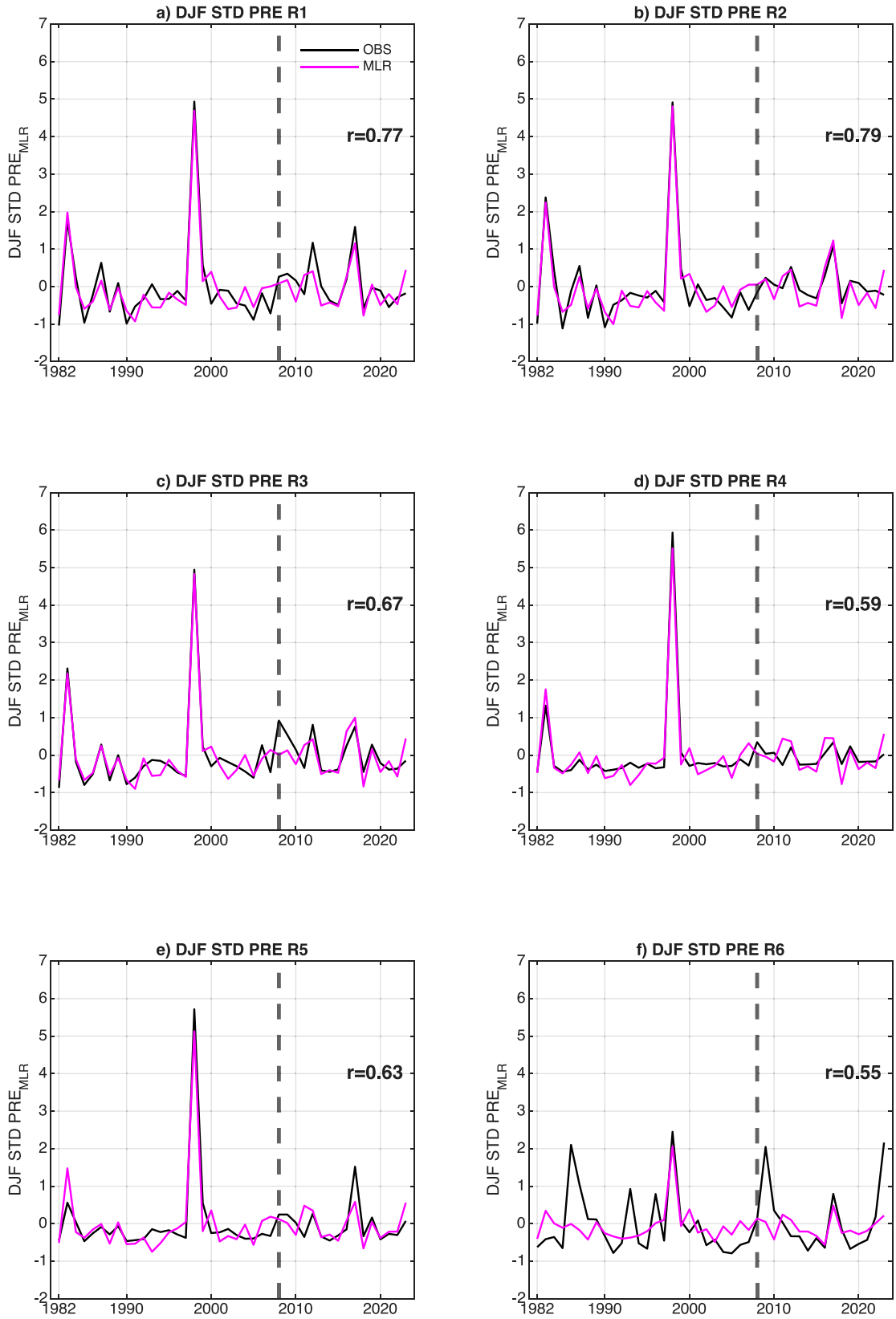

Figure 12. The observed (blue line) and estimated average DJF precipitation time series by the MLR_{OBS} model (red line) for six regions located within the western coast of South America: (a) the region R1, (b) the region R2, (c) the region R3, (d) the region R4, (e) the region R5, and (f) the region R6. The black numbers represent the correlation between observed and simulated by the MLR model in the testing period 2012–2023. The black and dashed line represents DJF 2006. The PISCOPv21 dataset was used in this analysis.

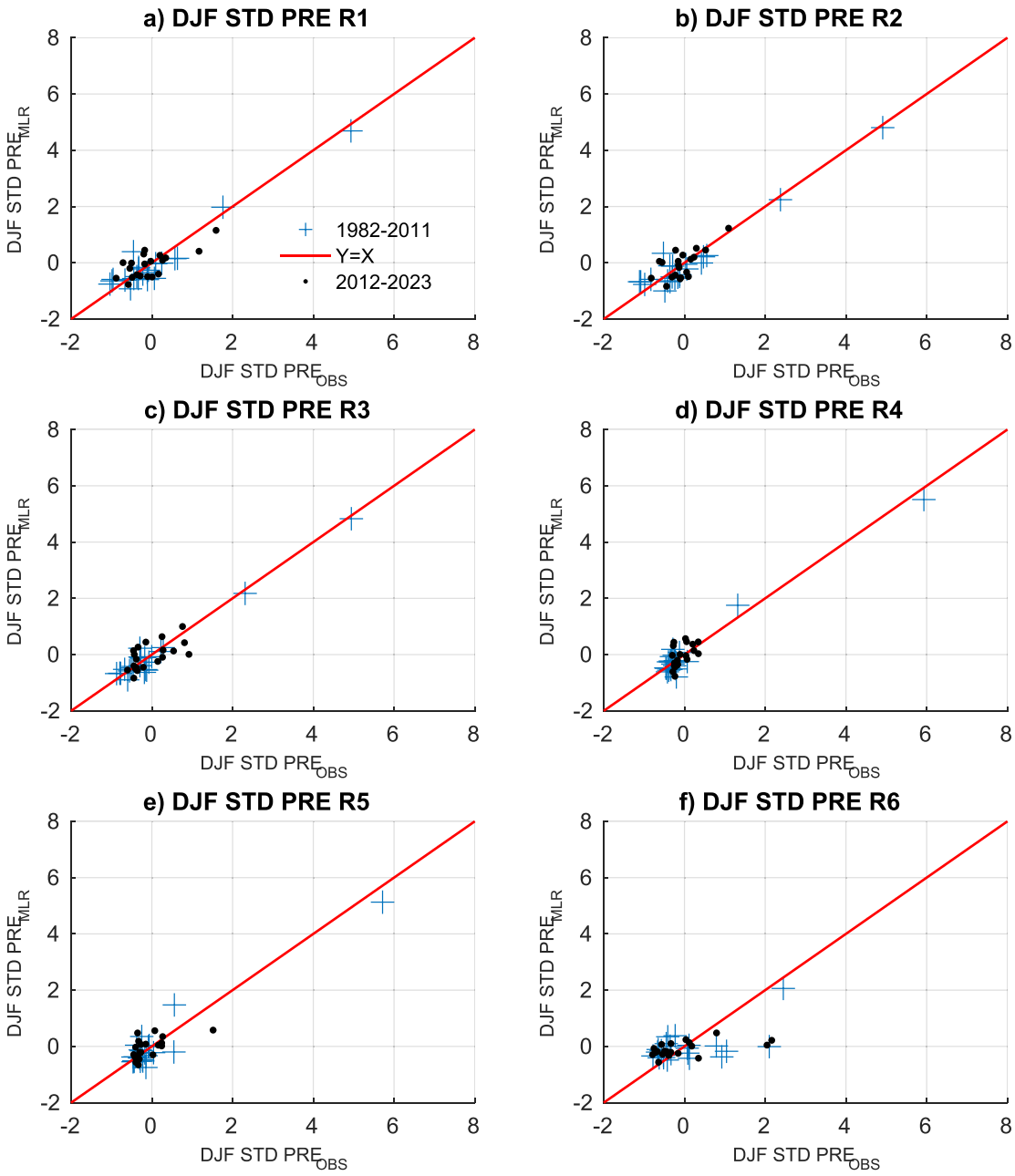

Figure 13. Scatterplot of observed and predicted DJF standardized precipitation anomalies in six regions located within western coast of South America: (a) the region R1, (b) the region R2, (c) the region R3, (d) the region R4, (e) the region R5 and (f) the region R6. The blue cross using the period 1982–2011. The black circles using the period 2012–2023. The red line represents the function identity (y = x). The analysis is based on the period 1982–2023.

Table 1. Multiple linear regression model (MLR_{OBS} and MLR_{PRED}) equation coefficients for estimating DJF standardized rainfall anomalies of the six regions (R1, R2, R3, R4, R5 and R6) within the western coast of South America (WCSA). Pearson and Spearman correlation coefficients and root-mean-square error (RMSE, in parenthesis) in standard deviation between observed and estimated time series of DJF rainfall anomalies of the six WCSA regions (R1, R2, R3, R4, R5 and R6) for the 2012–2023 testing period using observations and GFDL SPEAR forecasts as inputs. Significant correlation coefficients at 95% confidence level are shown in bold.

	MLR equation coefficients (1982–2023)					Corr. (RMSE)	
Region	Const.	E	C	CPITCZ	EPITCZ	Obs	Forecast
R1	−0.043	+0.31	0.0	**−0.48**	**+0.33**	**0.77/0.63** (0.37)	**0.76**/0.40 (0.59)
R2	−0.031	**+0.45**	0.0	**−0.46**	+0.27	**0.79/0.66** (0.30)	**0.72**/0.45 (0.55)
R3	0.027	**−0.37**	0.0	**−0.39**	**+0.37**	**0.67/0.71** (0.38)	**0.78**/0.57 (0.56)
R4	−0.0025	+0.1	0.0	**−0.36**	**+0.86**	**0.59/0.54** (0.29)	0.43/0.39 (0.71)
R5	−0.006	+0.17	0.0	**−0.43**	**+0.78**	**0.63/0.63** (0.36)	0.43/0.37 (0.76)
R6	−0.07	−0.16	0.0	−0.33	0.28	**0.55/0.55** (0.61)	0.48/**0.60** (0.66)

models is a cost efficient way to take advantage of the useful information produced by GCMs to predict precipitation in these regions. A previous study (Sulca *et al* 2018) showed that equatorial Pacific SST and precipitation indices can be used as inputs into a linear regression model to reproduce the austral summer precipitation in Peru, although they did not try to use forecast data as inputs. Consequently, this study focuses on developing a multiple linear regression (MLR) model for DJF precipitation forecasting on these coasts using observed and predicted indices of SST and precipitation (El Niño and ITCZ).

The results indicate that the Eastern Pacific El Niño SST (E), and the East Pacific ITCZ (EPITCZ) precipitation indices are positively correlated with the monthly precipitation along the northern Peru and Ecuador coasts, but are stronger in the E and EPITCZ indices, with the highest positive correlations with EPITCZ over the WCSA (figure 6). The positive correlation in these regions is maintained from October to February of the following year. In contrast, the Central Pacific El Niño SST (C) index presents a weak negative correlation with the WCSA precipitation from October to February of the following year. On the other hand, the Central Pacific ITCZ (CPITCZ) index presents a statistically significant negative correlation in this region only in January and February.

The GFDL-SPEAR model produces reasonable forecasts of the DJF SST variability in the eastern Pacific Ocean using December initial conditions, with strong and positive linear correlation between the observed and predicted time series of the E index, ($r > 0.7$, $p < 0.05$; figure 7(a)), as well as the large EPITCZ value during El Niño in 1998, although the remaining variability of the EPITCZ index is only moderately well reproduced, which is linked to the overestimation of the precipitation teleconnection over northern Peru (figure 8(d)) The correlations of the GFDL-SPEAR model forecasts for the DJF central Pacific El Niño SST (C) and CPITCZ indices with observations are also strong and statistically significant ($r > 0.70$, $p < 0.05$; figures 7(c), (d)), although the large negative CPITCZ value during El Niño in 1998 was underestimated.

In principle, the E index could be used to predict monthly precipitation over most of the WCSA, as it presents high correlations from October to February (figures 6(f)–(j)), consistent with Vavrus *et al*'s (2022) previous result, which pointed out that the efficiency of the CFSv2 model's forecasting of DJF precipitation over northwestern Peru is caused by the efficiency of the forecasting of the SST anomalies in the Niño1 + 2 region. However, several studies have reported that monthly SST anomalies in the eastern Pacific Ocean are not linearly related to monthly precipitation anomalies along the western coast of South America, as the linear relationship changes when these anomalies surpass a critical threshold (Woodman 1998, Jauregui and Takahahsi 2018, Takahashi and Martínez 2019).

Our results show that, when we also consider precipitation-based indices as potential predictors in a multiple linear regression model, these are assigned larger weight than the SST-based indices. Particularly, the EPITCZ index outperforms the E index in predicting DJF precipitation at each grid point within the WCSA in the context of our model, probably reflecting the stronger physical connection between the WCSA precipitation and the EPITCZ precipitation than with the SST-based E index. On the other hand, the larger weight that CPITCZ has relative to the C index most likely reflects a more direct causality link between central Pacific convection to the remote negative effects on precipitation via teleconnections (figures 5(b), (c)).

We tested the MLR_{OBS} model in the six clusters along the northern Peru and Ecuador coasts and found that performs well because the E, CPITCZ and EPITCZ indices correlate with the DJF precipitation across the WCSA. However, it presents a lower skill for the southwestern Piura and the northernmost Lambayeque (R4) and southern Lambayeque and northwestern La Libertad (R5), possibly due to a stronger reliance on the EPITCZ index (table 1), which was not well forecasted by the GCM during the testing period (figure 7(d)). The lower skill for the central part of western La Libertad (R6) regions likely caused by its weak connection to the change of the equatorial Pacific SST anomalies (figure 4(f)). The highest RMSEs are observed along the southwestern most and central-western coast of Ecuador, which would be associated with the lack of other regional and orographic precipitation forcings (Peñaranda-Vélez *et al* 2024) in the architecture of the MLR model.

A priori, the main limitation of the MLR model for forecasting DJF precipitation anomalies across WCSA would be the low GCM forecast skill for the EPITCZ index during moderate El Niño conditions. Additionally, the MLR model does not utilize other local precipitation-relevant predictors in its construction, such as thermodynamic indices (Rivas 2023) and tropical convection indices (Galvez and Davison 2016, Yu and Zhang 2018), the coastal El Niño (Takahashi *et al* 2018) or/and the combination of them (Mayta *et al* 2024), which could be relevant for the reduction of the bias of the MLR model (Manzanas and Gutiérrez 2019). The MLR model has some limitations in predicting the SON precipitation anomalies in the WCSA, as these are not primarily driven by changes in large-scale circulation anomalies over South America, unlike DJF precipitation anomalies, which respond to variations in the Eastern Pacific El Niño and the central and eastern Pacific ITCZ (CPITCZ and EPITCZ). The limited precipitation observed in WCSA before the austral summer results from arid conditions between July and November (Rau *et al* 2017, Ilbay-Yupa *et al* 2021).

Finally, the improved predictions of DJF precipitation anomalies along the coast of northern Peru and Ecuador using the MLR model may serve as input to enhance forecast-based actions to mitigate the impacts of droughts and floods in the region (Caramanica *et al* 2020, Lala *et al* 2021). Furthermore, this new tool could allow us to understand the impacts of climate change on WCSA precipitation and its predictability by explaining the

near-future change of the variability of the Eastern Pacific El Niño and the East Pacific ITCZ (Geng *et al* 2022). In addition, the identification of new remote teleconnection for the austral summer WCSA precipitation such as the cold phase of the Atlantic Meridional mode and the Tibetan Plateau thermal forcing, which intensify humidity flux from the Amazon basin (Chiang and Vimont 2004, Xie *et al* 2023, Affram *et al* 2024; Zhang *et al* 2024), may help to improve the current version of the MLR model. Furthermore, the enhanced Orinoco low-level jet and the cold phase of the Pacific Meridional mode — that intensifies the northerly and westerly moisture flux from the western tropical North Atlantic and the far-eastern Pacific (Chiang and Vimont 2004, Martinez *et al* 2022) — may also play a relevant role. These westerly and easterly moisture flux forcings could be used to develop a new moisture-transport-based MLR model to predict DJF WCSA precipitation in futures studies.

Acknowledgments

JS and KT acknowledge funding from the Peruvian PPR 068 program 'Reducción de Vulnerabilidad y Atención de Emergencia por Desastres'. This work was subsidized by CONCYTEC through the PROCIENCIA Program under the framework of the contest 'Scholarships in educational doctorate programs through inter-institutional partnerships', according to contract No. PE501093367-2024] and the Interinstitutional Alliances Contest for Doctoral Programs corresponding to the UNIVERSIDAD NACIONAL DE INGENIERIA, according to contract PE501084296-2023- PROCIENCIA-BM.

Conflict of interest

The authors declare that the research was conducted without any commercial or financial relationships that could be construed as a potential conflict of interest.

Data availability statement

All data that support the findings of this study are included within the article (and any supplementary files).

Author contributions

JS: Conceptualization, Formal analysis, Methodology, Software, Validation, Visualization, Writing—revised draft. KT: Formal analysis, Methodology, Validation, Visualization, Writing—revised draft.

Funding

JS and KT were funded by Peruvian PPR 068 program 'Reducción de vulnerabilidad y atención de emergencias por desastres'. JS was also funded by the Consejo Nacional de Ciencia, Tecnología e Innovación Tecnológica (CONCYTEC) and the Programa Nacional de Investigación Científica y Estudios Avanzados (PROCIENCIA) within the framework of the competition E033-2023-01-BM 'ALIANZAS INTERINSTITUCIONALES PARA PROGRAMAS DE DOCTORADOS, contract (PE501093367-2024-PROCIENCIA-BM).'

Code availability

The processing codes used in this study are available from the corresponding authors upon request.

References

Adler R F *et al* 2003 The version 2 global precipitation climatology project (GPCP) monthly precipitation analysis (1979-present) *J. Hydrometeor.* **4** 1147–67

Affram G, Zhang W, Hari V, Gao S, Ratterman C, Zhu L and Gillies R R 2024 Modulation of the pacific meridional mode on the dipole pattern of the CONUS summertime precipitation *Geophys. Res. Lett.* **51** e2024GL109636

Akoglu H 2018 User's guide to correlation coefficents *Turk. J. Emerg. Med.* **18** 91–3

Arthur D and Vassilvitskii S 2007 K-means++: the advantages of careful seeding *SODA 7: Procceding of the Eighteenth Annual ACM-SIAM Symp. on Discrete Algorithms* pp 1027–35

Ashok K, Behera S K, Rao S A, Weng H and Yamagata T 2007 El Niño Modoki and its possible teleconnection *J. Geophys. Res.* **112** C11007

Aybar C, Fernández C, Huerta A, Lavado W, Vega F and Felipe-Obando O 2020 Construction of a high-resolution gridded rainfall dataset for Peru from 1981 to the present *Hydrol. Sci. J.* **65** 770–85

Bayr T, Dommenget D, Martin T and Power S B 2014 The east-ward shift of the Walker circulation in response to global warmingand its relationship to ENSO variability *Clim. Dyn.* **43** 2747–276
Bazo J, Lorenzo M D L N and Da Rocha R P 2013 Relationship between monthly rainfall in NW Peru and the tropical sea surface temperature *Adv. Meteorol.* **2013** 152875
Beaton R H and Tukey J W 1974 The fitting of power series, meaning polynomials, illustrated on band-spectroscopic data *Technometrics* **16** 147–85
Bourrel L, Rau P, Dewitte B, Labat D, Lavado W, Coutaud A, Vera A, Alvarado A and Ordoñez J 2014 Low-frequency modulation and trend of the relationship between ENSO and precipitation along the northern to centre Peruvian Pacific coast *Hydrol Process* **29** 1252–66
Cai W, Santoso A, Collins M, Dewitte B, Karamperidou C, Kug J S and Zhong W 2021 Changing El Niño–Southern oscillation in a warming climate *Nat. Rev. Earth Environ.* **2** 628–44
Cai W, Wang G, Dewitte B, Wu L, Santoso A, Takahashi K, Yang Y, Carréric A and McPhaden M J 2018 Increased variability of Eastern Pacific El Niño under greenhouse warming *Nature* **564** 201–6
Capotondi A, Wittenberg A T, Kug J S, Takahashi K and McPhaden M J 2020 ENSO diversity *El Niño Southern Oscillation in a Changing Climate* ed M J McPhaden, A Santoso and W Cai ch 4 pp 65–86
Capotondi A, Wittenberg A T, Newman M, Di Lorenzo E, Yu J Y, Braconnot P and Yeh S W 2015 Understanding ENSO diversity *Bull. Am. Meteorol. Soc.* **96** 921–38
Caramanica A, Huaman-Mesia L, Morales C R, Huckleberry G, Castillo L J and Quilter J 2020 El Niño resilence farming on the north coast of Peru *PNAS* **117** 24127–37
Chiang J C H and Vimont D J 2004 Analogous pacific and atlantic meridional modes of tropical atmosphere–ocean variability *J. Clim.* **17** 4143–58
De Guenni L B, García M, Muñoz Á G, Santos J L, Perugachi C, Cedeño A and Castillo J 2017 Predicting monthly precipitation along coastal Ecuador: ENSO and transfer function models *Theor. Appl. Climatol.* **129** 1059–73
Delworth T L *et al* 2020 SPEAR: the next generation GFDL modeling system for seasonal and multidecadal prediction and projection *J. Adv. Model. Earth Syst.* **12** e2019MS001895
Ding H, Newman M, Alexander M A and Wittenberg A T 2018 Skillful climate forecasts of the tropical Indo-Pacific Ocean using model-analogs *J. Clim.* **31** 5437–59
Ding H, Newman M, Alexander M A and Wittenberg A T 2020 Relating CMIP5 model biases to seasonal forecast skill in the tropical Pacific *Geophys. Res. Lett.* **47** e2019GL086765
DuMouchel W H and O'Brien F L 1989 Integrating a robust option into a multiple regression computing environment *Computer Science and Statistics/Proc. 21st Symp. on the Interface* (American Statistical Association) pp 297–302
Falk R and Miller N 1992 *A Primer for Soft Modeling* (The University of Akron Press)
Fernandez-Palomino C A, Hattermann F F, Krysanova V, Lobanova A, Vega-Jácome F, Lavado W, Santini W, Aybar C and Bronstert A 2021 A novel high-resolution gridded precipitation dataset for Peruvian and Ecuadorian watersheds—development and hydrological evaluation *J. Hydrometeorol.* **23** 309–36
Galvez J M and Davison M 2016 The Gálvez-Davison index for tropical convection https://wpc.ncep.noaa.gov/international/gdi/ (Accessed 20 February 2024)
Geng T *et al* 2022 Emergence of changing Central-Pacific and Eastern-Pacific El Niño-Southern Oscillation in a warming climate *Nat. Comun.* **13** 6616
Gutierrez J M, Cano R, Cofiño A S and Sordo C 2005 Analysis and downscaling multi-model seasonal forecast in Peru using self-organizing maps *Tellus* **57A** 435–47
Huaman L and Schumacher C 2018 Assessing the vertical latent structure of the east Pacific ITCZ using the CloudSat CPR and TRMM PR *J. Clim.* **31** 2563–77
Huaman L and Takahashi K 2016 The vertical structure of the eastern Pacific ITCZs and associated circulation using the TRMM Precipitation Radar and *in situ* data *Geophys. Res. Lett.* **43** 8230–9
Ilbay-Yupa M *et al* 2021 Updating regionalization of precipitation in Ecuador *Theor. Appl. Climatol.* **143** 1513–28
Jauregui Y R and Takahahsi K 2018 Simple physical-empirical model of the precipitation distribution based on a tropical sea surface temperature threshold an the effects of climate change *Clim. Dyn.* **50** 2217–37
Kirtman B P *et al* 2014 The North American Multimodel ensmeble. Phase I seasonal-to-interannual prediction; Phase 2 toward developing intraseasonal prediction *Bull. Amer. Meteor. Soc.* **95** 585–601
Lagos P, Silva Y, Nickl E and Mosquera K 2008 El Niño—related precipitation variability in Perú *Adv. Geosc.* **14** 231–7
Lala J, Bazo J, Anand V and Paul Block P 2021 Optimizing forecast-based actions for extreme rainfall events *Clim. Risk Manag.* **34** 100374
Lavado-Casimiro W and Espinoza J C 2014 Impact of El Niño and La Niña on rainfall in Peru *Rev. Bras. Meteorol.* **29** 171–82
Llauca H, Lavado-Casimiro W, Montesinos C, Santini W and Rau P 2021 PISCO_HyM_GR2M: a model of monthly water balance in Peru (1981–2020) *Water* **13** 1048
Lu F *et al* 2020 GFDL's SPEAR seasonal prediction system: initialization and ocean tendency adjustment (OTA) for coupled model predictions *J. Adv. Model. Earth Syst.* **12** e2020MS002149
Manzanas R and Gutiérrez J M 2019 Process-conditioned bias correction for seasonal forecasting: a case-study with ENSO in Peru *Clim. Dyn.* **52** 1673–83
Martinez J A, Arias P A, Junquas C, Espinoza J C, Condom T, Dominguez F and Morales J S 2022 The Orinoco low-level jet and the cross-equatorial moisture transport over tropical South America: Lessons from seasonal WRF simulations *J. Geophys. Res. Atm.* **127** e2021JD035603
Mayta V C, Lin Q-J, Adames-Corraliza A F and Chavez-Mayta E 2024 Impact of tropical waves on extreme rainfall events during coastal El Niño *Env. Res. Lett.* **19** 094037
Peñaranda-Vélez V M, Quintanar A I, Ochoa-Moya C A and Vivoni E R 2024 An approach for modeling the orographic–forcing effect via random cascades and the long-term statistics of Mexico City's daily precipitation *J. Geophys. Res. Atm.* **129** e2023JD040023
Petrova D *et al* 2021 The 2018–2019 weak El Niño: predicting the risk of a dengue outbreak in Machala, Ecuador *Int. J. Climatol.* **41** 3813–23
Philander S G H, Gu D, Lambert G, Li T, Halpern D, Lau N-C and Pacanowski R C 1996 Why the ITCZ is mostly north of the Equator *J. Clim.* **9** 2958–72
Ratterman C, Zhang W, Affram G and Vernon B 2023 Improving the CFSv2 seasonal precipitation forecasts across the United States by combining weather regimes and Gaussian mixture models *J. Hydrometeor.* **24** 1583–93
Rau P, Bourrel L, Labat D, Melo P, Dewitte B, Frappart F, Lavado W and Felipe O 2017 Regionalization of rainfall over the Peruvian Pacific slope and coast *Int. J. Climatol.* **37** 143–58
Rayner N A, Parker D E, Horton E B, Folland C K, Alexander L V, Rowell D P, Kent E C and Kaplan A 2003 Global analyses of sea surface temperature, sea ice, and night marine air temperature since the late nineteenth century *J. Geophys. Res.* **108** 4407

Recalde-Coronel G C, Barnston A G and Muñoz A G 2014 Predictability of December-April rainfall in coastal and Andean Ecuador *J. Appl. Meteorol. Climatol.* **53** 1471–93
Ren H L *et al* 2019 Seasonal predictability of winter ENSO types in operational dynamical model predictions *Clim. Dyn.* **52** 3869–90
Rivas P R 2023 An index for predicting precipitation in the north coast of Peru using logistic regression *MS Thesis* University of Washington 92 https://digital.lib.washington.edu/researchworks/handle/1773/50209
Rivera-Tello G A, Takahashi K and Karamperidou C 2023 Explained predictions of strong eastern Pacific El Niño events using deep learning *Sci. Rep.* **13** 21150
Ropelewski C F and Halpert M S 1987 Global and regional scale precipitation patterns associated with the El Niño/Southern Oscillation *Mon. Weather Rev.* **115** 1606–26
Rossel F and Cadier E 2009 El Niño and prediction of anomalous monthly rainfalls in Ecuador *Hydrol. Proc.* **23** 3253–60
Sanabria J, Bourrel L, Dewitte B, Frappart F, Rau P, Solis O and Labat D 2018 Rainfall along the coast of Peru during strong El Niño events *Int. J. Climatol.* **38** 1737–47
SENAMHI 2023 Escenario probabilístico de lluvias - verano 2024. Informe técnico N° 10-2023/SENAMHI-DMA-SPC *SENAMHI* 11 https://repositorio.senamhi.gob.pe/bitstream/handle/20.500.12542/2917/Escenario-probabilístico-de-lluvias-verano-2024-Informe-Técnico-set_2023.pdf (Accessed April 19, 2024)
Srinivas G, Vialard J, Liu F, Voldoire A, Izumo T, Guilyardi E and Lengaigne M 2024 Dominant contribution of atmospheric nonlinearities to ENSO asymmetry and extreme El Niño events *Sci. Rep.* **14** 8122
Sulca J 2021 Evidence of nonlinear Walker circulation feedbacks on extreme El Niño Pacific diversity: Observations and CMIP5 models *Int. J. Climatol.* **41** 2934–61
Sulca J, Takahashi K, Espinoza J-C, Vuille M and Lavado W 2018 Impacts of different ENSO flavors and tropical Pacific convection variability (ITCZ, SPCZ) on austral summer rainfall in South America, with a focus on Peru. *Int. J. Climatol.* **38** 420–35
Sulca J, Vuille M, Elison-Timm O, Dong B and Zubieta R 2021 Empirical-statistical downscaling of austral summer precipitation over South America, with a focus on the central Peruvian Andes and the equatorial Amazon basin *J. Appl. Meteorol. Climatol.* **60** 65–85
Takahashi K 2004 The atmospheric circulation associated with extreme rainfall events in Piura, Peru, during the 1997–1998 and 2002 El Niño events *Ann. Geophys.* **22** 3917–26
Takahashi K *et al* 2018 The 2017 coastal El Niño [in 'State of the Climate in 2017'] *Bull. Amer. Meteor. Soc.* **99** S210–1
Takahashi K and Battisti D S 2007 Processes controlling the mean tropical Pacific precpitation pattern. Part I: the Andes and the Eastern Pacific ITCZ *J. Clim.* **20** 3434–51
Takahashi K and Dewitte B 2016 Strong and moderate nonlinear El Niño regimes *Clim. Dyn.* **46** 1627–45
Takahashi K and Martínez A G 2019 The very strong coastal El Niño in 1925 in the far-eastern Pacific *Clim. Dyn.* **52** 7389–415
Takahashi K, Montecinos A, Goubanova K and Dewitte B 2011 ENSO regimes: reinterpreting the canonical and Modoki El Niño *Geophys. Res. Lett.* **38** L10704
Thielen D *et al* 2021 Eventos hidroclimáticos extremos que afectan al embalse Daule-Peripa (Costa de Ecuador)—Dinámica histórica y teleconexiones *Rev. Climatol.* **21** 127–45 https://dialnet.unirioja.es/servlet/articulo?codigo=9414732
Thielen D R *et al* 2023 Effect of extreme El Niño events on the precipitation of Ecuador *Nat. Hazards Earth Syst. Sci.* **23** 1507–27
Tobar V and Wyseure G 2018 Seasonal rainfall patterns classification, relationship to ENSO and rainfall trends in Ecuador *Int. J. Climatol.* **38** 1808–19
Tran-Anh Q and Taniguchi K 2018 Coupling dynamical and statistical downscaling for high-resolution rainfall forecasting: case study of the Red River Delta, Vietnam *Prog. Earth Planet Sci.* **5** 28
Trenberth K E, Branstator G W, Karoly D, Kumar A, Lau N and Ropelewski C 1998 Progress during TOGA in understanding and modeling global teleconnections associated with tropical sea surface temperatures *J. Geophys. Res.* **103** 14291–324
Van der Wiel K, Matthews A J, Joshi M M and Stevens D P 2016 The influence of diabatic heating in the South Pcaific convergence zone on Rossby wave propagation and the mean flow *Q. J. R. Meteorol. Soc.* **142** 901–10
Vavrus S J, Wang F and Block P 2022 Rainy season precipitation forecasts in coastal Peru from the North American Multi-Model Ensemble *Int. J. Climatol.* **42** 6221–34
Waylen P R and Caviedes C N 1986 El Niño and annual floods on the north Peruvian littoral *J. Hydrol.* **89** 141–56
Wolter K and Timlin M S 1993 Monitoring ENSO in COADS with a seasonally adjusted principal component index *Proc. of the 17th Climate Diagnostics Workshop* (Univ. of Oklahoma) pp 52–7 https://psl.noaa.gov/enso/mei/ Norman, OK, NOAA/NMC/CAC, NSSL, Oklahoma Clim. Survey, CIMMS and the School of Meteor
Woodman R 1997 Análisis del Pronóstico del fenómeno de El Niño evacuado por NCEP/NOAA el 03 de diciembre de 1997: impacto sobre las lluvias en la costa norte del pais *IGP - Instituto Geofísico del Perú* 1–5 https://hdl.handle.net/20.500.12816/399
Woodman R 1998 Pronóstico de lluvias basado en los pronósticos de TSM de NOAA/NCEP: Ciudad de Piura *IGP—Instituto Geofísico del Perú* 1–5 http://hdl.handle.net/20.500.12816/589
World Bank 2014 *Financial Protection Against Natural Disasters: From Products to Comprehensive Strategies* (The World Bank) https://financialprotectionforum.org/publication/financial-protection-against-natural-disasters-from-products-to-strategies-an
Xie Y *et al* 2023 Oceanic repeaters boots the global climatic impact of the Tbetean Plateau *Sci. Bull.* **68** 2225–35
Yu H and Zhang M 2018 Explaining the year-to-year variability of the eastern Pacific Intertropical Convergence Zone in the boreal spring *J. Geophys. Res. Atm.* **123** 3847–56
Zhang Y *et al* 2024 Near-global summer circulation response to the spring surface temperature anomaly in Tibetan Plateau-the GEWEX/LS4P first phase experiment *Clim. Dyn.* **62** 2907–24
Zhao M *et al* 2018a The GFDL global atmosphere and land model AM4. 0/LM4.0: 1. Simulation characteristics with prescribed SSTs *J. Adv. Model. Earth Syst.* **10** 691–734
Zhao M *et al* 2018b The GFDL global atmosphere and land model AM4. 0/LM4.0: 2. Model description, sensitivity studies, and tuning strategies *J. Adv. Model. Earth Syst.* **10** 735–69
Zhou S, Huang G and Huang P 2020 Excessive ITCZ but negative SST biases in the tropical Pacific simulated by CMIP5/6 models: the role of the meridional pattern of SST bias *J. Clim.* **33** 5305–16